MASTERARBEIT | MASTER'S THESIS

Titel | Title

Characterization of NK cells in Mucosal Immunity: Insights from the Human Lung and Gut

verfasst von | submitted by

Julia Schaden BSc

angestrebter akademischer Grad | in partial fulfilment of the requirements for the degree of

Master of Science (MSc)

Wien | Vienna, 2024

Studienkennzahl lt. Studienblatt | Degree programme code as it appears on the student record sheet:	UA 066 834
Studienrichtung lt. Studienblatt | Degree programme as it appears on the student record sheet:	Masterstudium Molekulare Biologie
Betreut von | Supervisor:	Dr. Nicole Marquardt

Statutory Declaration

Hereby, I, Julia Schaden, declare that I have authored this Master's thesis independently, that I have not used other than the declared sources / resources, and that I have explicitly marked all material which has been quoted either literally or by content from the used sources.

I declare that this Master's Thesis has not been presented before.

Stockholm, July 2024

Eidesstattliche Erklärung

Ich, Julia Schaden, erkläre hiermit, dass ich die vorliegende Masterarbeit selbstständig verfasst, andere als die angegebenen Quellen/Hilfsmittel nicht benutzt und die den benutzten Quellen wörtlich oder inhaltlich entnommenen Stellen als solche kenntlich gemacht habe.

Diese Masterarbeit wurde bisher keiner anderen Prüfungsbehörde vorgelegt.

Stockholm, Juli 2024

Acknowledgements

We sincerely thank the patients, donors, and their families for consenting to participate in this research, as well as the surgeons and collaborators whose efforts made this study possible.

I would also like to thank Nicole Marquardt, our team leader and my supervisor, who gave me the opportunity to learn advanced techniques in the field of immunobiology, trusted me to work on my own projects and provided me with her constructive feedback on my thesis.

Special thanks also go to Nici Wild, our PhD student, who took on many responsibilities within our team and who was always ready to help others with persistent patience. Nici's support was crucial, especially for my work on the organoid project, and I greatly value the knowledge I gained from her.

I also thank Elena Bonaiti for her valuable help despite being so new to our team as well as Sophia Hald for teaching me a lot about microscopy. I also appreciate the friendships and support from my fellow master's colleagues and friends Camille Guédé, Fabian Zoppelt, Andréa Revillot, Marta Merlo, Niki Throumpari, Nadine van der Schaft, Sanne Eeckhout, and others.

Special thanks also go to Jack, not only for his scientific advice but also for his consistent support and belief in me during challenging times.

Lastly, my family's support throughout my studies has been invaluable.

Table of contents

Table of Contents

List of figures and tables

List of figures

List of tables

Abbreviations

B	
BALT	Bronchus-associated lymphoid tissue
BSA	Bovine serum albumin
C	
CD	Cluster of differentiation
CRC	Colorectal cancer
E	
EGF	Epidermal growth factor
F	
FcεRIγ	High-affinity immunoglobulin epsilon Fc region receptor I gamma chain
FcγRIII	Low-affinity immunoglobulin gamma Fc region receptor III
G	
GALT	Gut-associated lymphoid tissue
GCDR	Gentle Cell Dissociation Reagent
GI	Gastrointestinal tract
GzmA/B/K	Granzyme A/B/K
H	
HCMV	Human cytomegalovirus
I	
IBD	Inflammatory bowel disease
IEC	Intestinal epithelial cell
IFN	Interferon
IL	Interleukin
ILC	Innate lymphoid cell
ITAM	Immunoreceptor tyrosine-based activation motif
ITIM	Immunoreceptor tyrosine-based motif
K	
KIR	Killer immunoglobulin-like receptor
L	
LLT1	Lectin-Like Transcript 1
M	
MALT	Mucosa-associated lymphoid tissue
MFI	Mean fluorescence intensity
MHC	Major histocompatibility complex
min	Minute(s)

N

NK	Natural killer
NKRP1A	Natural killer receptor protein 1A
NSCLC	Non-small cell lung cancer

P

PBMC	Peripheral blood mononuclear cell
pbNK	Peripheral blood NK
PD1	Programmed cell death 1

R

RORγt	RAR-related orphan receptor gamma 2
RT	Room temperature

S

S1P	Sphingosine-1-phosphate
S1P1	Sphingosine-1-phosphate receptor 1
SARS-CoV-2	severe acute respiratory syndrome coronavirus 2
SCLC	Small cell lung cancer

T

T-bet	T-box expressed in T cells
T_{CM}	Central memory T cells
T_{EM}	Effector memory T cells
T_{EMRA}	Terminally differentiated effector memory T cells
Th	T helper
TIGIT	T cell immunoreceptor with Ig and ITIM domains
TIM3	T-cell immunoglobulin and mucin-domain containing 3
TNF	Tumor necrosis factor
TRAIL	TNF-related apoptosis-inducing ligand
trNK	Tissue-resident NK

Abstract

The mucosa of the respiratory and gastrointestinal tract is continuously exposed to a wide array of antigens, some of which can cause disease. Natural killer (NK) cells, crucial components of the innate immune system, are dispersed throughout the body, including peripheral tissues like the lungs and intestines. This thesis explores the different immune cell subsets and their functions in these tissues, with a focus on NK cells in the human lung and the human gut.

In the human lungs, received from organ donors, we identified distinct immune cell populations across eight anatomical regions using spectral flow cytometry for detailed immunophenotyping. T cells, particularly $CD4^+$ T cells, were the most abundant, highlighting their role in lung immunosurveillance. Tissue-resident memory T cells (T_{RM}) were identified throughout the lung, with highest frequencies of $CD4^+$ T_{RM} in the lower right parenchyma. NK cells were present in all lung regions and associated tissues, with $CD16^-$ NK cells predominating in lung-lymph nodes and the primary bronchus, and $CD16^+$ NK cells more common in parenchymal sites. In the lung parenchyma, tissue-resident NK (trNK) cells, defined by their expression of CD69, CD49a and/or CD103, constituted 24-37% of the $CD16^-$ subset. Within the $CD16^-$ population of two donors, we also identified adaptive-like $CD16^-CD49a^+$ NK cells, which have been previously described by the group.

In the gut, we elucidated the phenotype of human blood NK cells and $CD8^+$ T cells upon co-culture with patient-matched intestinal organoids generated from ileum and colon in order to investigate the interaction between intestinal tissues and NK cells in a more physiological context *in vitro*. Using 29-colour flow cytometry, we assessed phenotypic characteristics, including the expression of effector molecules, as well as degranulation and cytokine production by NK cells upon co-culture with intestinal organoids. As indicated by increased cell size, co-culture with ileal organoids potentially lead to NK and $CD8^+$ T cell activation. Moreover, decreased expression of effector molecules such as granzymes and perforin could be observed within NK and $CD8^+$ T cells, indicating that gut tissue might modulate immune cell activity. These findings highlight the importance of the intestinal microenvironment in shaping NK cell responses and potential implications for intestinal diseases such as inflammatory bowel disease (IBD).

Overall, this thesis provides a detailed characterization of NK cells in mucosal tissues such as the human lung and gut, contributing to our understanding of tissue-specific immune regulation and offering insights for therapeutic strategies in respiratory and gastrointestinal diseases.

Zusammenfassung

Die Schleimhaut der Atemwege und des Magen-Darm-Trakts ist kontinuierlich einer Vielzahl von Antigenen ausgesetzt, von denen einige Krankheiten verursachen können. Natürliche Killerzellen (NK-Zellen), wesentliche Komponenten des angeborenen Immunsystems, sind im gesamten Körper verteilt, einschließlich peripherer Gewebe wie Lunge und Darm. Diese Arbeit untersucht die verschiedenen Untergruppen von Immunzellen und ihre Funktionen in diesen Geweben, mit einem besonderen Fokus auf NK-Zellen in der menschlichen Lunge und im menschlichen Darm.

In den Lungen von Organspendern identifizierten wir mittels spektraler Durchflusszytometrie zur detaillierten Immunphänotypisierung unterschiedliche Immunzellpopulationen in acht anatomischen Regionen. T-Zellen, insbesondere $CD4^+$ T-Zellen, waren am häufigsten vertreten, was ihre potentielle Rolle in der Immunüberwachung der Lunge unterstreicht. Geweberesidente T-Gedächtniszellen (T_{RM}) wurden in der gesamten Lunge und lungeassoziierten Geweben identifiziert, mit der höchsten Frequenz von $CD4^+$ T_{RM} im Parenchym des unteren rechten Lungenflügels. NK-Zellen waren in allen Lungenregionen vorhanden, wobei $CD16^-$ NK-Zellen in den Lymphknoten und dem Hauptbronchus überwogen, während $CD16^+$ NK-Zellen häufiger in parenchymalen Bereichen vorkamen. Im Lungenparenchym machten geweberesidente NK (trNK)-Zellen 24 bis 37% der $CD16^-$ Untergruppe aus. Innerhalb der $CD16^-$ Population zweier Spender identifizierten wir auch adaptive $CD16^-CD49a^+$ NK-Zellen, die bereits zuvor von unserer Gruppe beschrieben wurden.

Im Darm untersuchten wir den Phänotyp von NK-Zellen und $CD8^+$ T-Zellen nach der Inkubation mit Darm-Organoiden, um die Interaktion zwischen Darmgewebe und NK-Zellen in einem physiologischeren Kontext *in vitro* zu untersuchen. Mithilfe von 29-Farben-Durchflusszytometrie charakterisierten wir die Expression von Effektormolekülen sowie die Degranulation und Zytokinproduktion von autologen Blut-NK-Zellen nach Kokultur mit menschlichen Darm-Organoiden. Eine Vergrößerung der Lymphozyten wies darauf hin, dass die Kokultur mit Ileum-Organoiden zur Aktivierung von NK- und $CD8^+$ T-Zellen führte. Zudem konnte eine verringerte Expression von Effektormolekülen wie Granzymen und Perforin bei NK- und $CD8^+$ T-Zellen beobachtet werden. Diese Ergebnisse unterstreichen den Einfluss der Darm-Mikroumgebung auf NK-Zellantworten und die potenziellen Auswirkungen auf Krankheiten wie chronisch-entzündliche Darmerkrankungen (IBD).

Insgesamt bietet diese Arbeit eine detaillierte Charakterisierung der NK-Zellen in mukosalen Geweben wie der menschlichen Lunge und dem Darm und trägt zum Verständnis der gewebespezifischen Immunregulation bei, was Einblicke für therapeutische Strategien bei Atemwegs- und Magen-Darm-Erkrankungen ermöglicht.

1. Introduction

1.1. Human NK cells

NK cells were initially identified in the 1970s in mice and characterized as “killer”-lymphocytes capable of targeting and destroying virally infected and/or malignant cells through their cytotoxic activities[1–3]. NK cells are crucial players in the innate immune system and were the first subtype to be identified among innate lymphoid cells (ILCs). Traditionally, they are characterized as lymphocytes that offer innate immune surveillance against both virally-infected cells and tumor cells by releasing cytolytic mediators and cytokines[4]. NK cells, along with other ILC family members, including type 1, 2, and 3 ILCs (ILC1s, ILC2s, and ILC3s) share a common lymphoid progenitor with T and B cells before branching off into their distinct lineages[3,5,6]. ILC1s and NK cells belong to the group 1 ILCs, known for their production of interferon-γ (IFN-γ) and their reliance on the transcription factor T-bet. Despite their developmental distinctiveness, discerning between NK cells and ILC1s can be challenging due to the overlap in their features and characteristics[7]. Although NK cells share the ability to produce IFN-γ with ILC1s, they also release lytic lysosomes containing perforin and granzymes, phenotypically resembling cytotoxic $CD8^+$ T cells[6]. NK cells are equipped with a diverse array of inhibitory and activating receptors, enabling them to recognize specific ligands present on the membranes of other cells (Figure 1).

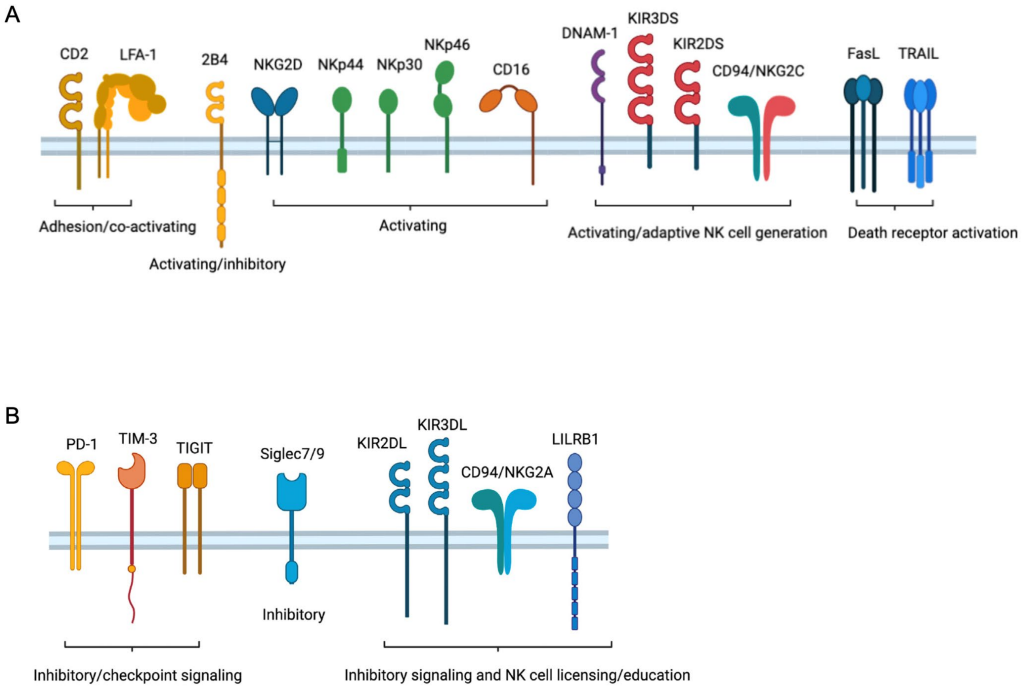

Figure 1. NK cell activating and inhibitory receptors. (A) Costimulatory receptors, activating receptors, and apoptosis-inducing death receptors expressed by NK cells. (B)Inhibitory receptors and checkpoint proteins expressed by NK cells. Figure adapted from Mace et al., 2023[8].

The delicate equilibrium between these inhibitory and activating signals ultimately determines the fate of the target cell, whether it will be spared or eliminated by the NK cell's potent cytotoxic abilities[9,10]. A variety of inhibitory receptors contribute to the establishment of immunological self-tolerance, while also initiating negative-feedback mechanisms to counter the activating signals initiated by activating receptors[11]. NK cells express a diverse array of inhibitory receptors, with their corresponding ligands predominantly belonging to the class I HLA molecules, such as HLA-A, HLA-B, HLA-C, and HLA-E. Many of these inhibitory receptors feature intracellular domains containing immunoreceptor tyrosine-based inhibition motifs (ITIMs). These motifs provide docking sites for membrane-proximal phosphatases, which cause a dampening in the signaling of activating receptors within NK cells. Among the most important examples of inhibitory receptors in NK cells are members of the killer immunoglobulin-like receptor (KIR) family, which bind to HLA-A, HLA-B, and HLA-C. Another prominent inhibitory receptor is CD94/NKG2A, which provides a binding site for HLA-E[11,12]. Furthermore, checkpoint inhibitors like programmed cell death 1 (PD1), T cell immunoreceptor with Ig and ITIM domains (TIGIT) and T-cell immunoglobulin and mucin-domain containing 3 (TIM3) seem to play a role in NK cell inhibition[13–15].

The expression of HLA class I proteins can be downregulated upon viral infection or malignant transformation. Once downregulated, the inhibitory receptors on NK cells lack their usual ligands, leading to NK cell activation. This mechanism, known as the "missing-self" hypothesis, describes the classic model of NK cell activation[16,17]. Moreover, NK cells express activating receptors that initiate signaling cascades upon their crosslinking and subsequent phosphorylation of their immunoreceptor tyrosine-based activation motifs (ITAMs)[9]. The most potent one is the low-affinity immunoglobulin gamma Fc region receptor III (FcγRIII), also known as CD16. It binds to the Fc regions of IgG antibodies on opsonized cells and thereby leads to the activation of the NK cell and the killing of the target cell upon crosslinking. This process is also referred to as antibody-dependent cellular cytotoxicity (ADCC)[9,10]. Additional receptors inducing NK cell activation include members of the natural cytotoxicity family, such as NKp30, NKp40, NKp44, and NKp46, which directly bind to virus-, bacteria- as well as tumor-associated antigens, inducing cytokine production and elimination of the target cell[18]. NKG2C and NKG2D are further activation receptors expressed by NK cells. NKG2C stimulates a signaling cascade upon dimerization with CD94 and subsequently binding to HLA-E, a ligand that is usually associated with inhibitory signaling as described above[19,20]. In addition to the above-mentioned receptors, cytokines such as IL-12, IL-15, or IL-18 can lead to stimulation of NK cells, that in turn start secreting proinflammatory IFN-γ and tumor necrosis factor alpha (TNF-α)[21].

NK cells are distributed throughout both the bloodstream and diverse tissues of the human body. So far, studies have mostly been focusing on peripheral blood NK cells, whereas their localization and function across different human tissues has been an emerging field of interest over the past decade. In the subsequent sections of this thesis, the latest insights into tissue-specific subsets of NK cells will be examined.

1.1.1. Human NK cells in blood

In peripheral blood, NK cells constitute around 15% of the circulating lymphocytes[22,23]. Generally, human NK cells can be characterized by the expression of CD56 and the absence of CD3[24]. Human NK cells are typically categorized into two main subsets: $CD56^{dim}$ and $CD56^{bright}$. $CD56^{dim}$ cells constitute about 90% of NK cells in peripheral blood and exhibit high levels of CD16 expression, while the remaining 10% comprise $CD56^{bright}$ NK cells which generally lack CD16 expression [22]. Moreover, some of the $CD56^{dim}CD16^{+}$ NK cells express KIR and CD57, which serve as markers for terminally differentiated $CD56^{dim}$ NK cells but are not expressed by $CD56^{bright}CD16^{-}$ NK cells[23,25,26].

$CD56^{bright}CD16^{-}$ NK cells are known for their capatcity to rapidly produce proinflammatory cytokines such as IFN-γ and TNF upon stimulation, whereas $CD56^{dim}CD16^{+}$ NK cells demonstrate higher cytotoxicity towards infected and malignant cells by releasing granules containing granzyme B (GzmB) and perforin across the immunological synapse. However, under activating conditions both subsets can secrete cytolytic granules as well as cytokines[8]. Subsequently, during serial killing, they engage death receptors such as Fas ligand and TNF-related apoptosis-inducing ligand (TRAIL)[21,27–29].

Although $CD56^{dim}CD16^{+}$ NK cells are more frequent in peripheral blood, $CD56^{bright}CD16^{-}$ NK cells have been identified in various tissues like lymph nodes, tonsils, liver, and intestines where they might have important roles for the immune system[30–32]. In the following chapters of this thesis, NK cells and their roles in human tissues will be discussed.

1.1.2. NK cells in tissues

NK cells are dispersed across the human body, not only found in the blood as well as primary and secondary lymphoid organs but also in peripheral tissues including the intestines, lungs, liver, skin, and uterus[23,33–37]. Most of the current knowledge about NK cells is based on studies in peripheral blood which are referred to as peripheral blood NK (pbNK) cells. However, recent research has increasingly shed light on the less-explored population of trNK cells present in different peripheral tissues[35,38]. Compared to NK cells in peripheral blood, trNK cells share the expression of specific integrins, i.e. CD49a and CD103 as well as CD69 which all play a crucial role in retaining lymphocytes in tissues and therefore serve as defining hallmarks for tissue residency[23,39].

CD69 is a marker that is functionally involved in the inhibition of sphingosine-1-phosphate receptor 1 (S1P1), which interacts with sphingosine-1-phosphate (S1P). S1P, in turn, is a signaling sphingolipid that forms a gradient, with highest concentrations in the blood and therefore leads to egress of lymphocytes from tissue sites into peripheral blood by binding to its receptor S1P1. Inhibition of S1P1 by CD69 therefore causes lymphocytes, including trNK cells, to be retained in tissues[40,41]. Several studies have reported that NK cells residing in different human tissues such as liver, skin, uterus, intestines, and lymph nodes show high expression of CD69 compared to those present in peripheral blood[23,39,42–45].

Another hallmark marker for tissue-residency is CD49a, also known as α1 integrin, which is forming a heterodimer with β1 integrin that binds to collagen IV[46]. Collagen IV is commonly found in the basement membrane, a type of extracellular matrix lining the basal side of epithelial and endothelial cells[47]. Therefore, the expression of CD49a ultimately leads to the retention of the cell in tissues. Human NK cells expressing CD49a have been found for example in the liver and tonsils[43,46,48].

Additionally, the expression of CD103, also called αE integrin, facilitates tissue-residency by forming a heterodimer with β7 integrin and subsequently binding to E-cadherin expressed by epithelial cells[49,50]. TrNK cells expressing CD103 could for example be observed in the salivary glands[51].

Up to this point, trNK cells have exclusively been identified as $CD56^{bright}CD16^{-}$ NK cells. It is suggested that their role primarily involves maintaining tissue homeostasis rather than common NK cell functions such as the release of cytotoxic proteins. Moreover, although trNK cells share certain hallmark proteins for retainment within tissue-sites, they exhibit differences and tissue-specific traits potentially influenced by their microenvironments[23,39]. Further research needs to be conducted in order to gain more insights into the phenotypes and functions of organ-specific trNK cells. In the following chapters, a focus is set on NK cells residing in human intestinal as well as lung tissue.

1.1.3. NK cells in healthy tissues

1.1.3.1. Lung

Situated at the environmental interface, the mucosa of the human lung is regularly subjected to foreign antigens like microorganisms and external particles. This exposure often causes inflammatory conditions such as microbial infections, allergies, asthma as well as cancer[52]. In order to maintain the delicate equilibrium between tolerating harmless particles and fighting invading pathogens, a specialized microenvironment within the lung tissue is crucial. This microenvironment comprises the respiratory epithelium and a network of non-circulating lung-resident immune cells, including tissue-resident T cells, B cells, alveolar macrophages, dendritic cells as well as ILCs and NK cells[53,54]. Analysis of

NK cells within healthy human lung tissues revealed the presence of distinct subsets distinguished by their expression of CD56 and NKp46[55]. In later studies, most NK cells being present in human lungs were found to express a highly differentiated phenotype, marked by $CD56^{dim}CD16^{+}$ expression, and demonstrated decreased responsiveness to target cell stimulation[36]. Interestingly, the majority of these NK cells do not express the tissue-residency marker CD69, indicating that they primarily circulate rather than reside within the lung. However, it was also shown that a significant portion of $CD56^{bright}CD16^{-}$ NK cells found in the lung do express CD69[52]. Additionally, other studies detected a functional and potentially lung tissue-resident NK cell subset with a $CD49a^{+}CD103^{+}CD69^{+}$ phenotype in the parenchyma of lung explants. This subset seemed to respond to viral infection by degranulation[56]. Furthermore, inhibition of NK cell recruitment from peripheral blood into the lungs does not affect the ability of NK cells to control tumor growth. This does not only indicate the presence but also the significance of lung tissue-resident NK cells[57]. It was also shown that, upon infection with influenza, lung NK cells upregulate their expression of CD107a, IFN-γ and granzyme B, promoting an immune response and the killing of infected macrophages[56,58,59].

Moreover, a subset of NK cells, termed adaptive-like NK cells, has been identified in both lung tissue and blood[60]. These adaptive-like NK cells, also referred to as adaptive, memory, and memory-like NK cells, were initially observed in peripheral blood, where they exhibit a $CD56^{dim}CD16^{+}$ phenotype along with increased expression of KIRs, NKG2C, and CD57, a marker for NK cell maturation[61,62]. Furthermore, they are associated with human cytomegalovirus (HCMV) infections and, expand and contract upon repeated infections[63]. In the human lung, adaptive-like NK cells were characterized as $KIR^{+}NKG2C^{+}CD16^{-}$ and, in some donors, made up to 98% of $CD16^{-}$ NK cells[60]. They exhibited distinctive phenotypic features, notably a tissue-resident phenotype marked by the expression of CD69, CD49a, and/or CD103. These newly defined $CD16^{-}$ adaptive-like lung trNK cells further displayed 102 differentially expressed genes compared to $KIR^{-}NKG2C^{-}$ lung trNK cells. Moreover, individuals with adaptive-like $CD16^{-}$ NK cells in the lungs also harbored $CD16^{-}CD49a^{+}$ NK cells in their peripheral blood, referred to as adaptive-like $CD16^{-}CD49a^{+}$ pbNK cells. Regarding functionality, increased degranulation as well as production of TNF and IFN-γ, demonstrated in lung NK cells from donors with expansions of $CD16^{-}CD49a^{+}$ adaptive-like NK cells, suggested a hyperresponsiveness of these NK cells to target cells[60]. These findings indicate in vivo priming of NK cells, leading to enhanced functional responsiveness in the human lung and blood[60]. This heightened activity could make NK cells a promising candidate for cancer immunotherapies, particularly for targeting solid tumors.

Overall, the diverse subsets of NK cells identified within the human lung, including tissue-resident and adaptive-like NK cells, highlight the intricate immune landscape of this organ. These subsets exhibit unique phenotypic markers and functional features, suggesting specialized roles in immune surveillance and response within the lung microenvironment. The discovery of these distinct NK cell populations underscores their significance in lung immunity and presents promising outlooks for further research and therapeutic interventions targeting lung-related diseases such as lung cancer.

1.1.3.2. Gut

To fully understand how the body responds to environmental stimuli, it is essential to explore the role of the gut-associated lymphoid tissue (GALT). The GALT is a crucial component of the mucosa-associated lymphoid tissue (MALT) found throughout the gastrointestinal tract (GI). Given the constant exposure of the gut lumen to external substances, it is crucial for the GALT to discern between pathogenic and beneficial antigens[64,65]. As the first line of defense against pathogenic microorganisms, innate lymphocytes including NK cells and ILCs are playing an important role in executing and regulating immune responses within the gut[7,33,66]. Gut NK cells are dispersed across the epithelium and the stroma, where they interact with several other cell types such as macrophages, dendritic cells, T cells, fibroblasts as well as epithelial cells. They thereby maintain immune homeostasis and promote immune responses[64,67]. As a result, they play a crucial role in responding to intestinal infections, primarily by producing IFN-γ. This, in turn, triggers the recruitment of more NK cells from the bloodstream, amplifying systemic inflammation[64]. Moreover, NK cells are involved in the development of IBD including Crohn's disease (CD) and ulcerative colitis (UC), both of which increase the risk of colorectal cancer (CRC)[68–70].

While NK cells are found in the gut, it remains uncertain whether they are tissue-resident or originate from NK cells circulating in the peripheral blood[33,64]. However, NK cells in the peripheral blood do not exhibit expression of CCR6 or CCR9, chemokine receptors typically associated with the small intestine, indicating a lack of homing capability and thus suggesting tissue-residency of gut NK cells instead of derivation from peripheral blood NK cells[71–73]. In contrast, about 90% of NK cells in the peripheral blood express CD161, also referred to as natural killer receptor protein 1A (NKRP1A), a receptor that becomes upregulated following stimulation by IL-2[74,75]. This receptor is commonly found on most lymphocytes infiltrating the intestines as well as pbNK cells and ILCs[76,77]. Studies in $CD4^+$ T cells derived from peripheral blood have shown that CD161 acts as adhesion molecule and is involved in transendothelial migration[78]. Additionally, LLT1 (Lectin-Like Transcript 1), a ligand for CD161, has been found to be expressed in various human tissues such as intestines, and has been suspected to play a role in regulating NK cells and preventing

tissue damage[76]. Moreover, the stromal derived factor 1 (SDF1), also known as CXCL12, is a ligand expressed on NK cells binding to CXCR4 and thereby favoring tissue localization[79,80]. Taken together, these findings suggest the potential for peripheral blood NK cells to migrate into the gut. However, their precise origin and the specific adhesion molecules and chemokine receptors involved remain to be fully elucidated.

Furthermore, studies have demonstrated that NK cells are present in relatively low frequencies within the gastrointestinal (GI) tract compared to other tissues like the bone marrow, the spleen, and the lungs[30]. The majority of NK cells in the GI tract display an immature phenotype and belong to the $CD56^{bright}CD16^{-}$ subset, exhibiting diminished effector capacity such as reduced secretion of granzyme B and decreased expression of high-affinity IgE receptor (FcεRIγ), suggesting a lower ADCC capacity[30]. However, gut NK cells display tissue-resident features, including the expression of CD103 and the chemokine receptor CXCR6 as well as a decreased expression of S1PR1[30]. While mature and terminally differentiated NK cells seem to be largely absent from intestinal sites, specific subtypes of NK cells are predominantly maintained in the gut, distinct from those found in blood or other tissues. One such subtype co-expresses NKp44 and NKp46, resembling NK cell phenotypes associated with IBD[30,64].

In summary, these studies underline the potential involvement of NK cells in tissue-specific immune-regulatory functions within the GI. However, our understanding of NK cells and their roles in the gut and gut-associated diseases remains limited, necessitating further research to unravel their functions, particularly within distinct intestinal regions such as the ileum, caecum, and colon.

1.1.4. NK cells in tissue-specific pathologies

Given their immune-regulatory functions in mucosal tissues, NK cells also play crucial roles in both lung and gut-specific pathologies. Lung cancer, for example, is globally the primary cause of cancer-related death mortality and can be categorized into small-cell (SCLC) and non-small-cell cancer (NSCLC), whereas NSCLC makes up about 85% of all lung cancer cases[81–83]. NK cells play a key role in tumor immunosurveillance by detecting and killing malignant cells, highlighted by the increased vulnerability to cancer and metastasis observed in correlation with reduced NK cell activity[84,85]. NK cells are therefore crucial for tumor immunosurveillance in lung cancer. However, they exhibit compromised cytotoxicity and exhaustion in NSCLC due to the tumor microenvironment[86]. The immune checkpoint proteins PD-1 and CTLA-4 as well as factors such as hypoxia and elevated TGF-β levels contribute to this dysfunction[87–89]. Despite these challenges, understanding NK cell subsets in lung cancer could enhance therapeutic strategies.

Moreover, NK cells also play pivotal roles in respiratory infections such as influenza and severe acute respiratory syndrome coronavirus 2 (SARS-CoV-2). Influenza viruses annually cause global epidemics, infecting up to a billion people worldwide[90]. Although vaccines help in reducing transmission, they do not offer complete protection, and infection with influenza viruses as well as SARS-CoV-2 can result in significant inflammation and tissue damage[91]. While NK cells are crucial for detecting and eliminating cells infected with influenza virus[92,93], the specific role of circulating and tissue-resident NK cells at the primary infection site remains unclear regarding their contributions to the antiviral immune response and potential pathology[94]. During SARS-CoV-2 infections, a decline in peripheral blood NK cells has been reported as they migrate to the lungs[91,95]. Moreover, severe COVID-19 cases show an expansion of adaptive-like NK cells and altered NK cell receptor profiles, contributing to decreased cytotoxicity and complex interactions within the lung microenvironment[96,97]. Understanding NK cell behavior in these infections is essential for developing therapies to mitigate tissue damage within the human lung.

IBD, as a term for UC and CD, manifests as chronic inflammation in the gut, affecting distinct regions such as the ileum in CD and primarily the colon and rectum in UC. Both conditions involve excessive production of pro-inflammatory cytokines, yet their precise immunological causes remain unclear[98,99]. Genetic studies highlight the significance of KIR polymorphisms in IBD, with associations found between specific KIR genes and the development of UC and CD[100]. Variations in NK cell subsets, such as decreased NKp44$^+$ NK cell frequencies in CD and altered expression of NKG2D in UC, suggest their involvement in disease pathogenesis[101–104]. Further investigation into NK cell roles in IBD is crucial due to these complexities and the potential implications for therapeutic strategies.

In summary, NK cells play pivotal roles in human lung and gut tissues, influencing various tissue-specific diseases. From their involvement in tumor surveillance in lung cancer to their response during respiratory infections like influenza and SARS-CoV-2, as well as chronic inflammation such as IBD, NK cells demonstrate crucial immune regulatory roles. However, their contributions are still not fully understood, highlighting the need for continued research to fully elucidate their roles within the human lung and gut biology, thereby unraveling their full potential for treatment of these diseases.

1.2. Analysis of tissue-resident NK cells

1.2.1. Intestinal organoids

Ever since the establishment of the HeLa cervical cancer cell lines in 1953, immortalized cancer cell lines have been extensively applied in researching cell physiology and cancer[105]. Advancements in stem cell biology have enabled the development of three-dimensional *in vitro* tissue cultures, commonly referred to as "organoids". These structures

consist of functional living cells that spatially organize themselves and possess the capacity for self-renewal, thereby reproducing the architecture of human tissue and overcoming limitations of standard cell lines[106]. These characteristics have rendered organoid cultures essential for both basic and translational research involving a wide range of human tissues, including small intestines, colon, stomach, liver, tongue, pancreas, lungs, heart, and skin, derived from stem cells or differentiated cells[106–116]. Sato *et al.* developed the predominant model of intestinal organoid culture system in 2009, introducing intestinal organoids as the first tissue-derived organoid type to be established[107]. This method involves culturing intestinal crypts in a collagen matrix supplemented with media containing the Wnt agonist R-spondin 1, epidermal growth factor (EGF), and Noggin, crucial components for sustaining long-term organoid culture[107]. These conditions lead to the organization of crypts into sealed units with a central lumen, whereas the apical side of the cells is facing the inside. These structures mimic crypt-like domains, harboring intestinal stem cells as well as villus-like domains populated by goblet cells, Paneth cells, enteroendocrine cells, and absorptive enterocytes, as illustrated in Figure 2[108].

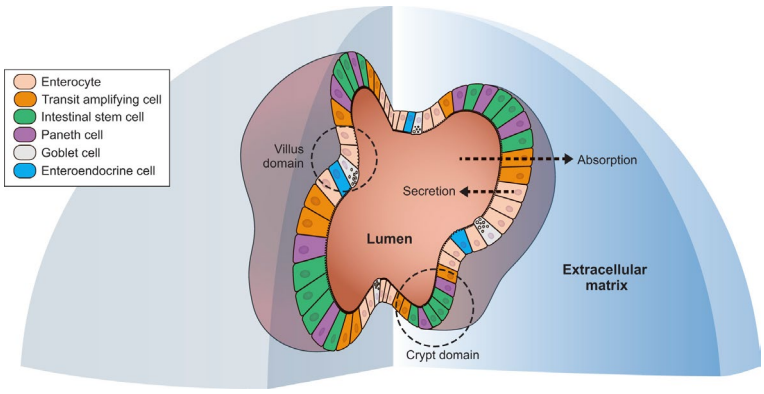

Figure 2. Structure of an intestinal organoid in extracellular matrix. Adapted from Almeqdadi et al., 2019[106].

Intestinal organoids do not only offer the possibility of studying intestinal physiology, cancer as well as host-microbe interactions and the embryonic development of the gut, but also allow to investigate the interplay between epithelial cells and the immune system, including lymphocytes[117,118]. T cell co-cultures with gut organoids have been explored in mouse models to investigate immune-epithelial interactions[117,119]. Similarly, co-culture systems have been developed to examine the interaction between macrophages and the intestinal mucosal barrier, aiming to understand host responses to enteric pathogens as well as regeneration upon inflammation[120,121]. ILCs and NK cells have been cocultured with intestinal organoids, yet the interaction between NK cells and human intestinal organoids remains largely unexplored[122,123].

Furthermore, research has been carried out on IBD, including UC and CD, utilizing human organoid models[124]. Interestingly, despite maintaining similar morphologies, organoids obtained from intestinal epithelial cells (IECs)u of IBD patients displayed DNA methylation signatures and transcription patterns that seemed to be specific for inflammatory bowel disease[125–127]. Gut organoids have been used as a model system to examine the functions of immune cells, such as macrophages and T cells, in IBD[128,129]. Based on co-cultivation of human intestinal organoids with NK cells, HLA-DP expressed on epithelial cells was shown to facilitate tissue damage by NKp44$^+$ NK cells in UC[123].

Overall, intestinal organoids serve as a valuable model system for investigating immune responses in the gut, not only in healthy tissue but also in diseases like IBD. So far, there have been only a few studies conducted on NK cells in intestinal organoid models. Further research is needed to understand the function of NK cells in the human gut, both in healthy and IBD contexts.

1.2.2. Spectral Flow Cytometry

Flow cytometry, widely employed across scientific disciplines, analyses scatter and fluorescence properties at the single-cell level to detect cellular properties and identify distinct cell subsets within a suspension. Whereas early cytometers in the 1970s allowed for the parallel analysis of two parameters, modern high-end flow cytometers are equipped with five to six lasers, facilitating the simultaneous analysis of approximately 30 parameters. Traditional flow cytometry records emitted photons from fluorophores within specific ranges of the light spectrum and applies compensation to mitigate spillover of emission spectra across detectors. However, the increase of fluorochromes also leads to an increase in the complexity of compensation matrices. The recently developed spectral flow cytometry offers a solution to these limitations, surpassing traditional flow cytometry methods[130–133].

Optical filters in traditional flow cytometry capture specific parts of the light spectrum corresponding to each fluorophore's peak emission. In contrast, spectral flow cytometry overcomes limitations inherent in traditional flow cytometry by recording the entire emission spectrum and using an unmixing algorithm to differentiate individual fluorochromes with similar emission peaks[132,134–136]. This innovative approach enables the incorporation of fluorophores with overlapping emission maxima into the same panel, expanding the range of protein markers analyzed simultaneously[134]. For example, the Cytek Aurora spectral flow cytometer, that has been used in this study, is equipped with 64 fluorescence detectors and five lasers, and allows for the analysis of up to 40 colors, potentially extending to 60 colors with its high number of detectors.

Moreover, spectral cytometers also extract autofluorescence spectra, enhancing signal-to-noise ratios and improving the resolution of dim markers that emit at similar wavelengths as the autofluorescence of the measured cells[132]. This capability is particularly beneficial in tissues with high autofluorescence levels, such as the heart, intestine, skin, and liver[132,133,137,138]. In contrast to traditional flow cytometry, spectral flow cytometry can differentiate minor cell subsets even in the presence of high autofluorescence or contamination by other cell types with different autofluorescence spectra[133]. By utilizing unique autofluorescence spectra, spectral flow cytometry enables the discrimination of distinct cell populations solely based on their autofluorescence fingerprints[135,139].

Despite extensive research on immune cells from human blood, our understanding of tissue-resident immune cells in the human body remains limited due to challenges like restrictions in the numbers of fluorochromes and therefore immunological markers that can be analyzed simultaneously[133,140–144]. Utilizing flow cytometry, the immune landscape within tissue microenvironments, primarily in murine models, encompassing organs such as the lung, gut, liver, spleen, skin, brain, kidney, and lymph nodes have been investigated[145,146]. Recent advancements in spectral flow cytometry have facilitated deeper exploration of tissue-resident immune cells in murine spleen, liver, skin, and mesenteric lymph nodes[133,147]. Insights gained from flow cytometry analyses of human tissues have proven valuable in understanding tissue-resident cell populations. These include NK cells, ILCs, B cells, $CD4^+$ T cells, and $CD8^+$ T cells, distributed across diverse solid organs such as the lung[60,148–150], intestines[151,152], liver[153,154], skin[155,156], spleen[157], and lymph nodes[158]. However, the utilization of spectral flow cytometry in human studies remains relatively understudied, with limited available data across organs[159–162].

Overall, spectral flow cytometry offers advanced analytical capabilities while simplifying compensation matrices, making it ideal for deep immunophenotyping of highly autofluorescent tissue-derived cell suspensions[133]. Nevertheless, across different human tissues, further studies remain to be undertaken.

2. Aims of the thesis

The primary aim of this thesis was to explore and decipher the different immune cell subsets and their potential functions across various human tissues, with a particular emphasis on NK cells in the human lung and gut.

In the human lung, we investigated and identified the distinct immune cell subsets present in different anatomical regions such as the primary bronchus, different sites of the lung parenchyma and lung-associated lymph nodes. Specifically, NK cells and their subsets were studied across these regions. For this, spectral flow cytometry was applied, which allowed for the use of a high number of fluorochromes and therefore the analysis of a broad range of markers, enabling detailed immunophenotyping and comprehensive analysis of the immune landscape.

In the human gut, we focused on elucidating the phenotype of NK cells and $CD8^+$ T cells. Here, we generated intestinal organoids from ileum and colon to study the interaction between intestinal tissues and NK cells in a more physiological context *in vitro*. Using 29-colour flow cytometry, we assessed phenotypic characteristics, including the expression of effector molecules, as well as degranulation and cytokine production by autologous blood NK cells upon co-culture with human intestinal organoids.

Overall, this thesis aimed at spatial identification and characterization of NK cell subsets at different sites in the human lung and gut, using primary cells as well as *in vitro* tissue models. The respective data will contribute to a deeper understanding in the regulation of NK cells within different human tissues.

3. Materials and Methods

3.1. Buffers and reagents

Buffers and reagents used throughout this study are summarized in Table 1.

SOLUTIONS/REAGENTS	COMPANY	PREPARATIONS
PBS	-	In-house production. Stored at RT.
R0 medium	-	RPMI (Gibco) 1640, supplemented with 100U/ml Penicillin (Invitrogen), 50ug/ml streptomycin (Invitrogen), 1mM L-glutamine (Invitrogen). Stored at 4°C.
R10 medium	-	RPMI 1640, supplemented with 10% heat-inactivated FCS (Thermo Scientific), 100U/ml Penicillin, 50µg/ml streptomycin, 1mM L-glutamine. Stored at 4°C.
FACS Wash buffer	-	1x PBS, supplemented with 2% heat-inactivated FCS and 2mM EDTA (Invitrogen). Stored at 4°C.
Collagenase type II	Sigma-Aldrich	Reconstituted in H_2O á 10mg/ml. Stored at -20°C. Stock concentration = 10mg/ml. Final concentration = 0.25mg/ml.
Dnase I	Roche	Reconstituted in H2O á 10mg/ml. Stored at -20°C. Stock concentration = 10mg/ml. Final concentration = 0.2mg/ml.
Accutase	Sigma-Aldrich	Stored at -20°C.
Lymphoprep™	STEMCELL Technologies	Stored at RT.
Trypan Blue Solution	Gibco	Used to determine live/dead cell ratio: 38µl trypan blue + 2µl cell suspension (1:20 dilution). 10µl added to the Neubauer chamber.
Türk's solution	Sigma-Aldrich	Used for cell counting: 38µl Türk's solution + 2µl cell suspension (1:20 dilution). 10µl added to the Neubauer chamber.

Zombie NIR™ Fixable Viability Kit	BioLegend	Reconstituted according to instructions. Diluted in 15µl PBS for usage (used at a dilution of 1:400 for staining in a total volume of 50µl).
LIVE/DEAD™ Fixable Aqua Dead Cell Stain Kit	Invitrogen	Reconstituted according to instructions. Used at a dilution of 1:100 for staining.
BD GolgiPlug™ (brefeldin A)	BD Biosciences	Stored at 4°C.
BD GolgiStop™ (monensin)	BD Biosciences	Stored at 4°C.
eBioscience™ Intracellular Fixation & Permeabilization Buffer Set	eBioscience	Fixation/Permeabilization concentrate diluted at a 1:4 ratio in Fixation/Permeabilization diluent. Permeabilization Buffer diluted 1:10 in distilled H2O.
Complete IntestiCult™ Organoid Growth Medium (Human)	STEMCELL Technologies	IntestiCult™ OGM Human Basal Medium and Organoid Supplement (both stored at -20°C) mixed at a 1:1 ratio. Antibiotics were added immediately before use.
Penicillin-Streptomycin	Invitrogen	Stock concentration = 10 000 U/ml Final concentration = 100 U/ml
Corning® Matrigel® Growth Factor Reduced (GFR) Basement Membrane Matrix, Phenol Red-free, LDEV-free	Corning	Stored at -20°C.
D-PBS (without Ca++ and Mg++)	Gibco	Stored at RT.
DMEM + 1% BSA	-	DMEM/F-12 with 15mM HEPES (Gibco), supplemented with 1% Bovine serum albumin (BSA; Sigma-Aldrich) in PBS. Stored at 4°C.
Gentle Cell Dissociation Reagent	STEMCELL Technologies	Stored at RT.
Y-27632 (Dihydrochloride)	STEMCELL Technologies	Reconstituted according to instructions. Stored at -20°C.
PBS-EDTA buffer	-	Per ml buffer, 20µl of 500 mM EDTA and 980µl of PBS

Table 1. List of reagents and buffers.

3.2. Human organ donor cohort

Human tissues from deceased organ donors were collected through the Immunology Human Organ Donor Programme (IHOPE). The inclusion criteria conformed to national

guidelines for organ donation and transplantation, with tissues not designated for transplantation being utilized for research purposes with the consent of the donor or next of kin. Deceased donors underwent routine serological testing for Hepatitis B surface and core antigens, Hepatitis C, HIV-1, cytomegalovirus, and syphilis. This study has been approved by the Swedish Ethical Review Authority (ID: 2019-05016 and 2021-00545).

3.3. Gut tissue collection

Gut tissues and patient-matched blood were collected from donors with our without ongoing inflammation undergoing planned colonoscopies through collaborators at the Capio Gastro Center Stockholm. The study has been approved by the Swedish Ethical Review Authority (ID: 2023-00840-01 and 2024-00594-02).

3.4. Healthy blood

Following the necessary approvals from the Swedish Ethical Review Authority (ID: 2006/229-31/3 and 2020-02604), peripheral blood samples for collection of internal control peripheral blood mononuclear cells (PBMCs) were obtained through buffy coats from healthy donors at the blood transfusion clinic at Karolinska University Hospital.

3.5. Lung tissue processing

After surgery, human tissues were transported to the research facilities where lung tissue was kept on ice and peripheral blood was stored at room temperature. Where required for logistical reasons, tissues and blood were stored overnight before processing. For processing, lung tissue was transferred to a metal dish and covered with PBS. The lung sections of interest were isolated and processed in 50ml tubes with R0 medium by cutting them into smaller fragments. Enzymatic digestion was performed using collagenase (0.25mg/ml) and DNase (0.2mg/ml) and incubating on a shaker at 37°C for 30min. After

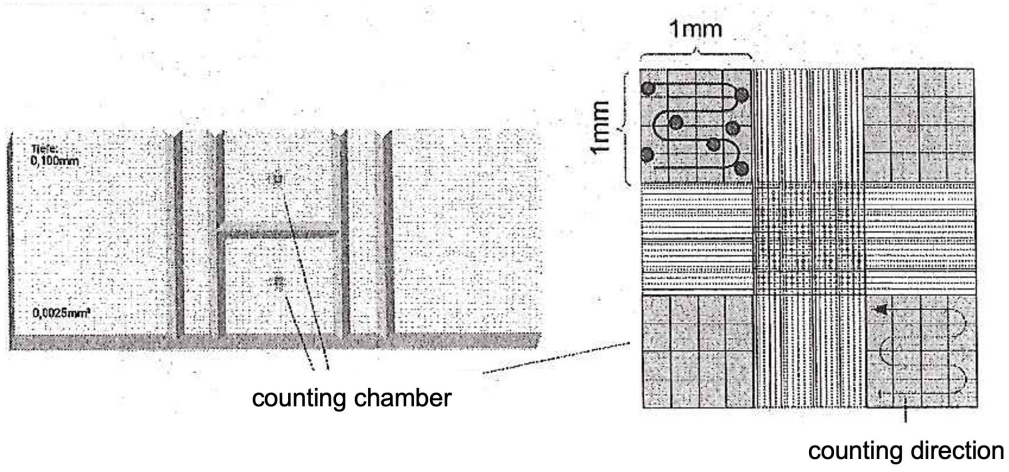

Figure 3. Graphical illustration of cell counting in counting chambers.

incubation, the digestion was stopped by diluting the tissue-R0 mix by at least 1:2 with R10 medium. In order to obtain cell suspensions, the samples were then filtered through 70µm and 40µm filters, followed by a centrifugation step (300 x g, 10min, RT). The cells were subsequently washed with PBS (800 x g, 7min for 15ml tubes or 800 x g, 10min for 50ml tubes) and then resuspended in 1ml FACS Wash buffer. Cell counts were performed in a Neubauer counting chamber as illustrated in Figure 3 by diluting cell suspensions in trypan blue and Türk's solution (cell count/number of squares x dilution factor x 10,000 = cells/ml). The cell concentrations were adjusted to 10 x 10^6 cells/ml in FACS Wash for downstream assays and spectral flow cytometry.

3.6. Isolation of human intestinal crypts from biopsies

For the isolation of human intestinal crypts from biopsies, the following steps were performed using sterile technique: Reagents including D-PBS (without Ca++ and Mg++) and DMEM + 1% BSA were placed on ice. Tissue samples, consisting of 4-5 biopsies per site (ileum and colon), were washed in a 15ml conical tube with 10ml of ice-cold PBS. After allowing the tissue to settle by gravity for approximately 10 seconds, the supernatant was removed. This washing step was repeated, leaving 1ml of supernatant in the tube. The tissue and the remaining supernatant were transferred to a 1.5ml microcentrifuge tube using a 1ml pipettor. The tissue was then thoroughly minced into the smallest pieces possible using sterile scissors and transferred to a new 15ml conical tube using a 1ml pipettor. The microcentrifuge tube was rinsed with PBS, and the rinse was added to the tissue fragments. The tissue fragments were allowed to settle by gravity for approximately 10 seconds before the supernatant was removed.

Next, 10ml of Gentle Cell Dissociation Reagent (GCDR) was added to the tissue fragments, and the mixture was incubated on ice on a rocking platform set at medium speed (~40 RPM) for 30min. After incubation, the sample was centrifuged at 300 x g for 5 minutes, and the supernatant was discarded. For the remainder of the protocol, pipette tips were pre-wetted with DMEM + 1% BSA to prevent crypts from sticking to the walls of the pipette tip. The tissue sample was then mixed with 1ml of ice-cold DMEM + 1% BSA and vigorously pipetted up and down 20 times with a 1ml pipettor to remove crypts from the tissue, while avoiding touching the sides or bottom of the tube with the pipette tip.

Finally, the contents of the tube were passed through a 70µm strainer into a new 50ml conical tube using a 1ml pipettor. The strainer was slightly tilted to ensure optimal passage of the crypts. The original tube was rinsed with 1ml of DMEM + 1% BSA, and the rinse was passed through the strainer into the new tube and pooled with the previously filtered crypt suspension. The isolated crypts were then ready for further processing and organoid culture.

3.7. Organoid culture from isolated human intestinal crypts

For organoid culture from isolated human intestinal crypts, the following steps were performed: First, 100µl of matrigel were thawed on ice, while a tissue culture-treated 24-well flat-bottom plate was pre-warmed in a 37°C incubator for at least two hours. Then, the total number of crypts in the sample was determined by placing 10µl aliquots of the sample on a Neubauer counting chamber. Using a bright-field microscope, the number of crypts in each 10µl aliquot was counted, as illustrated in Figure 4. In order to determine the total number of crypts in the 2ml sample, the crypt count was multiplied by 200. To obtain a yield of about 100-200 organoids per dome, 4000 crypts were seeded for each dome. After determining the total number of crypts per sample, the sample containing the desired number of crypts (here 8000 crypts) was centrifuged at 200 x g for 5min, and all but 50µl

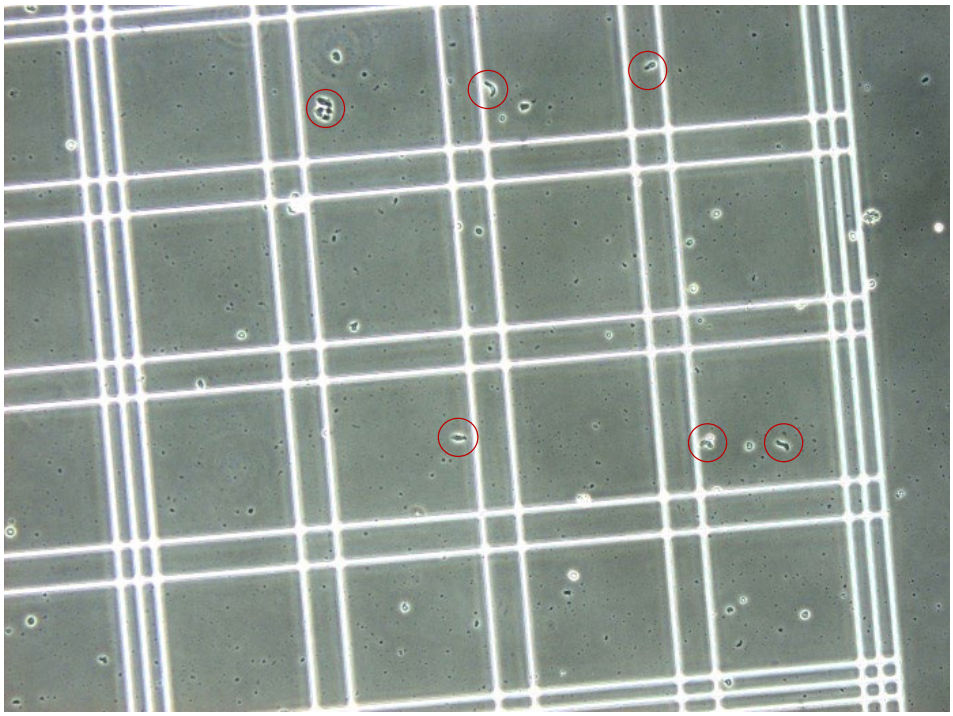

Figure 4. Example of human intestinal crypts (marked in red circles) isolated from biopsies in a Neubauer counting chamber. The image was taken in a bright-field microscope.

of but 50µl of the supernatant was removed. To prepare for plating, the 24-well plate was removed from the 37°C incubator, and a 200µl pipette tip was pre-wetted with DMEM + 1% BSA. Then, 50µl of the matrigel were added to the sample tube, and the pellet was resuspended thoroughly by pipetting up and down 10 times, while avoiding introducing bubbles. Using a pre-wetted 200µl pipette tip, 50µl of the matrigel-crypt suspension were drawn up and added to one of the eight central wells of the 24-well tissue culture-treated plate. The pipette was held vertically over the center of the well, and the suspension was carefully dispensed to form a dome. This process was repeated once, so all the matrigel-crypt suspension was dispensed. The plate was then carefully transferred to a 37°C

incubator and incubated for 10min to allow the domes to solidify without disturbance. Subsequently, 3ml of complete IntestiCult™ Organoid Growth Medium were prepared at RT supplemented with Penicillin-Streptomycin (100 U/ml), and for primary culture, 10µl of 3mM Y-27632 (Dihydrochloride) were added to achieve a final concentration of 10µM. After mixing thoroughly, 750µl of the prepared medium were added to each culture dome by gently dispensing along the wall of the well to avoid disturbing the domes. Sterile PBS was added to the unused wells in order to avoid evaporation of the medium. The culture plate was covered with its lid and incubated at 37°C and 5% CO_2. Every two days, a full medium change was performed using complete IntestiCult™ Organoid Growth Medium containing Penicillin-Streptomycin, and organoid growth was tracked in a bright-field microscope.

3.8. Preparation of human PBMCs from blood samples

For isolating PBMC from peripheral blood, the blood was transferred into a 50ml falcon tube, diluted 1:2 with PBS, and underlaid with Lymphoprep at a 1:3 ratio and centrifuged (800 x g, 20min, RT, low acceleration, no brake) in order to separate cell populations. The interphase containing the PBMCs was carefully collected and transferred into a fresh 15ml tube, which was then filled with PBS. For this first wash, the cells were centrifuged at 800 x g for 7min, the supernatant was discarded, and the cells were resuspended in 1ml of FACS Wash buffer. The cells were counted in a Neubauer chamber by diluting in trypan blue and Türk's solution, respectively, and subsequently, a second wash was conducted by centrifuging at 200 x g for 7min. The cells were resuspended in 1ml of freezing medium, consisting of FBS and 10% DMSO, and then frozen at -80°C before cryopreserving in liquid nitrogen until usage.

3.9. Coculture of natural killer cells and intestinal organoids

For cocultures of intestinal organoids and patient-matched PBMCs at 8-14 days after initiating the organoid culture, PBMCs were thawed and diluted in a total volume of 10ml R10 medium containing 10µg/ml DNase. After centrifugation at 500 x g for 5min at RT, the supernatant was discarded, and the cell pellet was resuspended in 1ml R10 medium. Cells were then counted, and 6 - 7.5 x 10^5 cells were cultured in 200µl R10 in a 96-well U-bottom plate at 37°C and 5% CO2. 10 ng/ml IL-15 were added for 3 hours of stimulation.

In order to harvest organoids, the organoid growth medium was removed from the wells, and 1ml of PBS-EDTA buffer was added to the domes to disrupt the matrigel by pipetting. The organoid suspension was then transferred to a sterile 2ml Eppendorf tube, and samples containing ileum or colon were pooled, respectively, followed by 30min incubation at 4°C to dissolve matrigel residues.

The organoids were then centrifuged at 480 x g for 4min to remove cell debris, and the supernatant was carefully removed by pipetting. PBMCs in R10 medium were added to the organoid pellet, resuspended and coculture was initiated, continuing for 16 hours at 37°C and 5% CO2 in a 96-well U-bottom plate. The same procedure was performed for the control sample, but without intestinal organoids present in the coculture.

After 16 hours of organoid-PBMC coculture, the organoid-PBMC mixture was transferred into a sterile 1.5ml Eppendorf tube and centrifuged at 480 x g for 4min to remove cell debris, with the supernatant carefully being discarded by pipetting. To harvest potentially infiltrated PBMCs, 1ml of GCDR was added to each well, followed by a 1-minute incubation at RT. The organoids were then vigorously pipetted up and down using a 1ml pipettor to disrupt them. After another 10min incubation with gentle agitation, the organoids were centrifuged at 200 x g for 5min, and the supernatant was discarded. The pellet was resuspended in 1ml of ice-cold DMEM/F-12 with 15 mM HEPES and centrifuged again at 200 x g for 5min. The supernatant was carefully aspirated, ensuring the pellet was not disturbed.

Next, 50µl of accutase were added to resuspend the organoids, and incubated at RT for 5-10min to achieve sufficient disruption into individual cells or small fragments, as confirmed by microscopic examination. Once dissociated, 50µl of DMEM/F-12 were added, and the mixture was pipetted up and down to mix thoroughly. The fragments were centrifuged at 200 x g for 5min, and the supernatant was carefully removed. Finally, the organoids were resuspended in 180µl of R10 medium and transferred into a V-bottom plate for further analysis.

3.10. Degranulation Assay

For the degranulation assay, PBMCs were cultured *in vitro*, with or without intestinal organoids, in presence of anti-human CD107a, brefeldin A (Golgi Plug), and monensin (GolgiStop) for a duration of 5 hours. Afterwards, a staining for multicolor flow cytometry was performed using the corresponding panel.

3.11. Extra- and intracellular staining protocol

After generating cell suspensions, the cells were transferred into a 96-well V-bottom plate at a concentration of 1-2 x 10^6 cells per well and then pelleted by centrifugation at 500 x g for 2 minutes. For spectral flow cytometry the cells were resuspended in 15µl of PBS containing the live/dead marker Zombie NIR (0,125µl DCM + 14,875µl PBS) and incubated in the dark at RT for 5min. This step was unique for spectral flow cytometry panels and not performed for conventional multicolor flow cytometry. Subsequently, 25µl of the chemokine receptor cocktail were added to each well, and the cells were resuspended and incubated

in the dark at 37°C with 5% CO2. After 10min, the remaining surface antibody cocktail was added in a volume of 25µl. Cells were resuspended and incubated for 15-20min at RT in the dark. This was followed by washing the cells by adding 120µl of FACS Wash buffer to each well, resuspending, centrifuging at 500 x g for 2min at RT, and discarding the supernatant. This washing step was repeated with 180µl of FACS Wash buffer.

For intracellular staining, cells were fixed by resuspending them in 200µl of Fixation/Permeabilization buffer and incubating for 20min at RT in the dark. Following fixation, the cells were centrifuged, the supernatant was removed, and the cells were resuspended in 180µl of Permeabilization Buffer. After another centrifugation step, cells were resuspended in 50µl intracellular antibody cocktail prepared in Permeabilization Buffer, resuspended and incubated for 20-30min at RT in the dark. If no intracellular staining was performed, samples were processed through the intracellular protocol without the addition of any intracellular antibodies to the Permeabilization Buffer in order to maintain consistency for internal comparisons. Finally, the cells were washed in 120µl of Permeabilization Buffer, followed by 180µl of FACS Wash buffer, and ultimately resuspended in 180µl of FACS Wash buffer. The cells were stored at 4°C until data acquisition on the flow cytometer. For data acquisition on the spectral flow cytometer, cells were filtered into 5ml tubes while they were transferred to 1.5ml cluster tubes for data acquisition on the conventional multicolor flow cytometer.

3.12. Spectral flow cytometry

Lung tissue was analyzed using spectral flow cytometry as described below.

3.12.1. Panel

The antibody panel and additional information for spectral flow cytometry are summarized in Table 2.

ANTIBODY TARGET	CLONE	FLUOROPHORE	COMPANY	DILUTION
CD1C	F10/21A3	BB700	BD Biosciences	1:100
CD3	UCHT1	Alexa Fluor 532	Invitrogen	1:50
CD4	SK3	Spark NIR 685	BioLegend	1:200
CD8	RPA-TB	BUV395	BD Biosciences	1:200
CD11C	B-ly6	BB515	BD Biosciences	1:200
CD14	S18004B	Spark YG 593	BioLegend	1:400
CD15	W6D3	BV750	BD Biosciences	1:50
CD16	3G8	cFluor V450	Cytek Biosciences	1:100

CD19	HIB19	BV510	BioLegend	1:100
CD20	2H7	PerCP	BioLegend	1:50
CD24	SN3	PE-AF610	Invitrogen	1:100
CD25	M-A251	PE-Dazzle 594	BioLegend	1:100
CD27	O323	BV785	BioLegend	1:400
CD38	HB-7	APC-Fire 810	BioLegend	1:400
CD45	HI30	BUV805	BD Biosciences	1:200
CD45RA	HI100	BV570	BioLegend	1:400
CD49a	SR84	BUV615	BD Biosciences	1:50
CD56	B159	BUV563	BD Biosciences	1:100
CD57	QA17A04	BV605	BioLegend	1:400
CD69	FN50	BUV737	BD Biosciences	1:200
CD71	M-A712	BUV661	BD Biosciences	1:100
CD83	HB15e	PerCP-eFluor 710	Invitrogen	1:50
CD86	2331 (FUN-1)	BB630-P2	BD Biosciences	1:400
CD95	DX2	PE-Cy5	BioLegend	1:200
CD103	Ber-ACT8	BB660-P2	BD Biosciences	1:100
CD117 (C-KIT)	104D2	BB755-P	BD Biosciences	1:400
CD123	6H6	SuperBright 436	Invitrogen	1:200
CD127	HIL-7R-M21	PE-Cy7	BD Biosciences	1:100
CD141	1A4	BV711	BD Biosciences	1:200
CD161	HP-3G10	BUV496	BD Biosciences	1:50
CD193 (CCR3)	5E8	R718	BD Biosciences	1:400
CD197 (CCR7)	G043H7	APC-Cy7	BioLegend	1:100
CX3CR1	2A9-1	PE	BioLegend	1:100
FCεRIα	AER-37	BV650	BD Biosciences	1:100
HLA-DR	L243	PE-Fire 810	BioLegend	1:100
IGD	IA6-2	Alexa Fluor 647	BioLegend	1:200
IGM	SPM557	DyLight 350	Novus Biologicals	1:50
KIR2DL1/S1	EB6	PC5.5	Beckman Coulter	1:100
KIR2DL2/L3/S2	GL183	PC5.5	Beckman Coulter	1:100
NKG2C	REA205	Vio Bright FITC	Miltenyi Biotec	1:400
PD1	EH12.2H7	BV421	BioLegend	1:50

RB780	B-ly4	CD21	BD Biosciences	1:400
TCR Vα7.2	3C10	APC	BioLegend	1:200
TCR γδ	B1	BV480	BD Biosciences	1:50

Table 2. Fluorophore-conjugated antibody panel for spectral flow cytometry analysis.

3.12.2. Instrument details and analysis

Samples were analyzed on a Cytek Aurora spectral flow cytometer equipped with five lasers (Cytek Biosciences), and data were analyzed using SpectroFlo (Cytek Biosciences) and FlowJo 10.10.0 (BD Biosciences).

3.13. Multicolor flow cytometry

The PBMC-intestinal organoid coculture was analyzed using multicolor flow cytometry as described below.

3.13.1. Panel

The antibody panel and additional information for multicolor flow cytometry are summarized in Table 3.

ANTIBODY TARGET	CLONE	FLUOROPHORE	COMPANY	DILUTION
EXTRACELLULAR				
CD3	UCHT1	PC5	Beckman Coulter	1:50
CD4	SK3	BV750	BD Biosciences	1:50
CD8	SK1	BUV737	BD Biosciences	1:50
CD14	M5E2	V500	BD Biosciences	1:100
CD16	3G8	BUV496	BD Biosciences	1:50
CD19	HIB19	V500	BD Biosciences	1:100
CD45	HI30	BUV805	BD Biosciences	1:25
CD49a	SR84	BUV615	BD Biosciences	1:100
CD56	NCAM16.2	BUV563	BD Biosciences	1:50
CD57	QA17A04	BV605	BioLegend	1:100
CD69	FN50	PE-CF594	BD Biosciences	1:50
CD103	Ber-ACT8	BUV395	BD Biosciences	1:50
CD107A	H4A3	BV785	BioLegend	0.75:100

NKG2A	Z199	PE	Beckman Coulter	1:50
NKG2C	REA205	Vio Bright	Miltenyi Biotec	1:50
KIR2DL1/S1	EB6	PC5.5	Beckman Coulter	1:50
KIR2DL2/L3/S2	GL183	PC5.5	Beckman Coulter	1:50
INTRACELLULAR				
GRANZYME A	CB9	Alexa Fluor 700	BioLegend	1:100
GRANZYME B	GB11	RB780	BD Biosciences	1:100
GRANZYME K	G3H69	PerCP-eFluor 710	Invitrogen	1:100
IFNγ	4S.B3	BV570	BioLegend	1:50
PERFORIN	δG9	BB755	BD Biosciences	1:100
TNF-α	MAb11	BV650	BioLegend	1:50

Table 3. Fluorophore-conjugated antibody panel for multicolor flow cytometry analysis.

3.13.2. Instrument details and analysis

Samples were analyzed on a BD FACSymphony A5, equipped with 5 lasers (BD Biosciences), and data were analyzed using FlowJo 10.10.0 (BD Biosciences).

3.14. Software

Spectral flow and multicolour flow cytometric data were acquired using SpectroFlo (Cytek Biosciences) and BD FACS Diva (BD Biosciences), respectively. Data were analyzed with FlowJo (version 10.10.10). GraphPad Prism (version 10.2.3 for Mac) was employed for graphical presentations and statistical analyses. Organoid annotation and image display were performed using ImageJ.

3.15. Statistical Analysis

GraphPad Prism 9 was used to perform statistical analyses including Friedman test, Dunn's multiple comparison test (patient-matched), Kruskal-Wallis test (unmatched) as well as Wilcoxon matched-pairs signed rank test (patient-matched).

4. Results

4.1. Characterization of the immunological landscape within the human lung

To map the different immune cell subsets across the human lung, lung donations were obtained from four different donors, aged between 42 and 68 years, all considered as healthy. Clinical as well as demographical details of the donors are summarized in Table 4. We isolated viable leukocyte populations from various anatomical sections of the lung enabling unprecedented spatial and temporal phenotypic analysis using spectral flow cytometry. A detailed overview of the anatomical lung sections investigated is presented in Figure 5A.

Lung donors	**n = 4**
Sex	f = 2, m = 2
Mean age (years)	54.5 (min = 42, max = 68)
Mean BMI (kg/m^2)	23.5 (min = 19.7, max = 27.3)
Blood type	A+ = 3, 0+ = 1
Smoking status	non-smoker = 2, former smoker = 1, active smoker = 1
COPD	no COPD = 3, COPD = 1
CMV IgG	neg = 0, pos = 4
HBsAG	neg = 4, pos = 0
Anti-HBc	neg = 4, pos = 0
Anti-HBs	neg = 3, pos = 1
Anti-HCV	neg = 4, pos = 0
Anti-HIV	neg = 4, pos = 0
Syphilis	neg = 3, pos = 1

Table 4. Clinical and demographical details of the donors included in the study. CMV = cytomegalovirus; HBsAG = Hepatitis B surface antigen; anti-HBc = Hepatitis B core antibody; anti-HBs = Hepatitis B surface antibody; Anti-HCV = Hepatitis C antibody; Anti-HIV = HIV antibody.

First, the landscape of distinct immune cell subsets, including neutrophils ($CD45^+CD14^-CD15^+CD16^+$), T cells ($CD45^+CD14^-CD3^+$), B cells ($CD45^+CD3^-CD14^-CD19^+CD20^+$), NK cells ($CD45^+CD3^-CD56^+$), and non-NK ILCs ($CD3^-CD127^+CD161^+$), was assessed in the human lung parenchyma, based on well-established markers. As a representative site, the middle right parenchyma (MR) was chosen. The gating strategy used to identify the respective subsets for this analysis is depicted in Figure 5B. The frequencies of these immune cell subsets within the $CD45^+$ population were quantified, illustrated in Figure 5C. The analysis revealed that of all populations analyzed, T cells were the most abundant immune cell subset in the MR, with significantly higher frequencies compared to neutrophils and non-NK ILCs. Within the T cell population, $CD4^+$ T cells were generally

more prevalent than $CD8^+$ T cells, suggesting a trend towards higher frequencies of $CD4^+$ T cells within the human lung (Figure 5C). Further delineation of the $CD4^+$ T cell subset identified various subpopulations, including naïve T cells ($CCR7^+CD45RA^+$), T_{EMRA} (terminally differentiated effector memory T cells; $CCR7^-CD45RA^+$), T_{EM} (effector memory T cells; $CCR7^-CD45RA^-$), and T_{CM} (central memory T cells; $CCR7^+CD45RA^-$). Among these subpopulations, T_{EM} and T_{CM} were more frequent, with $CD4^+$ T_{EM} cells being significantly more abundant compared to T_{EMRA} cells. In contrast, within the $CD8^+$ T cell subset, T_{EM} and T_{EMRA} were predominant, with T_{EM} cells significantly outnumbering naïve T cells (Figure 5C). Additionally, mucosa-associated invariant T (MAIT; $CD161^+V\alpha7.2^+$) cells were detected within both $CD4^+$ and $CD8^+$ T cell populations at low frequencies, with $CD8^+$ MAIT cells being more frequent than $CD4^+$ MAIT cells. Regulatory T cells (Tregs; $CD127^-CD25^+$) were identified within the $CD4^+$ T cell population, and γδ T cells (γδ TCR^+) within the $CD8^+$ T cell population, both at relatively low frequencies (Figure 5C). Overall, the distribution of these immune cell subsets appeared consistent across the different donors.

Within the B cell population, plasmablasts ($CD27^+CD38^+$) were present at very low frequencies, whereas IgD^+ B cells were more prevalent (Figure 5D). Among the non-NK ILCs, the majority were identified as ILC1s or ILC2s ($CD16^-CD117^-$), with a minor fraction belonging to the ILC3 ($CD16^-CD117^+$) subset (Figure 5E).

As we are particularly interested in lymphocytes such as NK cells as well as $CD8^+$ T cells and their tissue-resident subsets, we further analyzed T_{RM} ($CD69^+$, $CD49a^+$, and/or $CD103^+$) across four different anatomical lung regions: Primary bronchus, UR (upper right parenchyma), MR (middle right parenchyma), and LR (lower right parenchyma) (Figure 5C). Within the $CD4^+$ T_{RM} population, a significant difference was observed between the primary bronchus and LR, with higher frequencies in the LR. Conversely, the frequencies of $CD8^+$ T_{RM} cells appeared to decrease from the primary bronchus to the LR, although this trend did not reach statistical significance. Overall, a variation of the frequencies of $CD4^+$ and $CD8^+$ T_{RM} cells could be observed between the different donors.

Altogether, our comprehensive analysis revealed distinct distributions of immune cell subsets within the human lung, with T cells being the most abundant and significant regional variations in T_{RM}.

4.2. Distribution of NK cells and their subsets across different anatomical regions of the human lung

Following a broad characterization of the immune landscape in the human lung, with a particular focus on lymphocytes, we conducted a more detailed analysis of NK cells and respective relevant their subsets. This analysis focused on seven distinct lung tissue

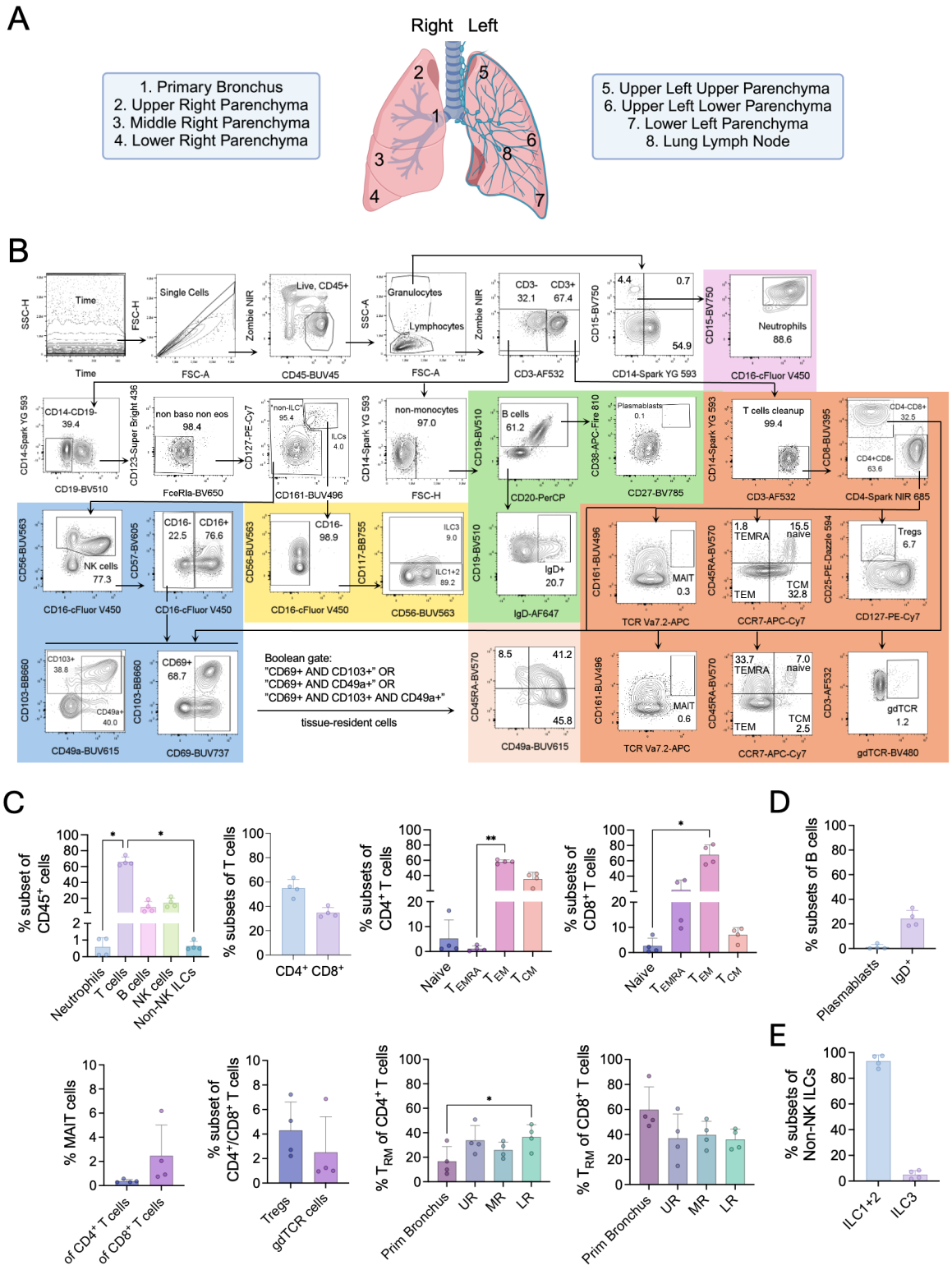

*Figure 5. Identification of immune cell subsets in the human lung. (A) Graphical overview of the investigated lung sections. Created with BioRender.com. (B) Gating strategy used for identification of the different immune cell subsets. Representative contours plots from MR of donor 1. (C) Summary of the frequencies of different immune cell subsets in MR (n=4). (D) Summary of the frequencies of CD4⁺ and CD8⁺ TRM T cells in different lung sections including Prim. Bronchus, UR, MR and LR (n=4). (C, D) Friedman test, Dunn's multiple comparison test (patient-matched), Wilcoxon matched-pairs signed rank test (patient-matched). *p < 0.05, **p < 0.01, ***p < 0.001, ****p < 0.0001.*

regions: Primary bronchus, UR, MR, LR, upper left upper parenchyma (ULU), upper left lower parenchyma (ULL), and lower left parenchyma (LL), as depicted in Figure 5A. In addition to lung tissue, lung-associated lymph nodes (LN) were included in our analysis.

Initially, we examined the distribution of NK cells (defined as $CD3^{-}CD56^{+}$) across these lung regions. NK cells were identified in all eight regions, with the highest frequencies observed in the lung parenchyma sections, ranging between 52-62% of $CD3^{-}$ cells (Figure 6A). In contrast, the primary bronchus and lung LN exhibited lower frequencies, with a significant difference noted between lung LN and UR.

Next, we quantified the $CD16^{-}$ and $CD16^{+}$ NK cell subsets within these regions. The lung LN and primary bronchus exhibited the highest frequencies of $CD16^{-}$ NK cells (54-78%), with a significant difference compared to UR (Figure 6B). In all parenchyma tissues, frequencies of $CD16^{-}$ NK cells were lower, ranging from about 22-33%.

Within the $CD16^{-}$ NK cell population, trNK cells were identified based on the expression of CD69, CD49a, and/or CD103 (gating strategy in Figure 5B). Frequencies of trNK cells ranged between 24% and 37% in the parenchyma regions, while the lung LN exhibited lower frequencies of this subset (Figure 6C). Interestingly, two outlier donors (donor 1 and 2) displayed particularly high frequencies of $CD16^{-}$ trNK cells as indicated in the representative plots as triangle and square data points (Figure 6C). This population expressed NKG2C, KIR as well as CD49a (Figure 6D), indicating the presence of $CD16^{-}$ $CD49a^{+}$ adaptive-like trNK cells which have been previously described by our group[60]. Adaptive-like $CD56^{bright}CD16^{-}$ NK cells, defined by the expression of NKG2C and KIR, were discovered in the human lung and blood, marked by tissue residency features such as CD49a expression. Lung adaptive-like trNK cells were hyperresponsive to target cells and were functionally distinct from nonadaptive $CD56^{bright}CD16^{-}$ lung trNK cells including higher expression of IFN-γ and lower levels of granzyme A (GzmA) and granzyme K (GzmK)[60]. Corresponding to these results, we could confirm the presence of adaptive-like trNK in the human lungs obtained by the organ donor cohort. $NKG2C^{+}KIR^{+}$ adaptive-like NK cells were also present among the $CD16^{+}$ NK cells within the same donors, but at much lower frequencies (Figure 6D).

Overall, detailed characterization of NK cells across different lung regions highlighted the presence of diverse NK cell subsets, including tissue-resident and adaptive-like NK cells, with no differences in frequencies between lung parenchyma tissues but larger differences between lung parenchyma and airway-associated tissue and LN.

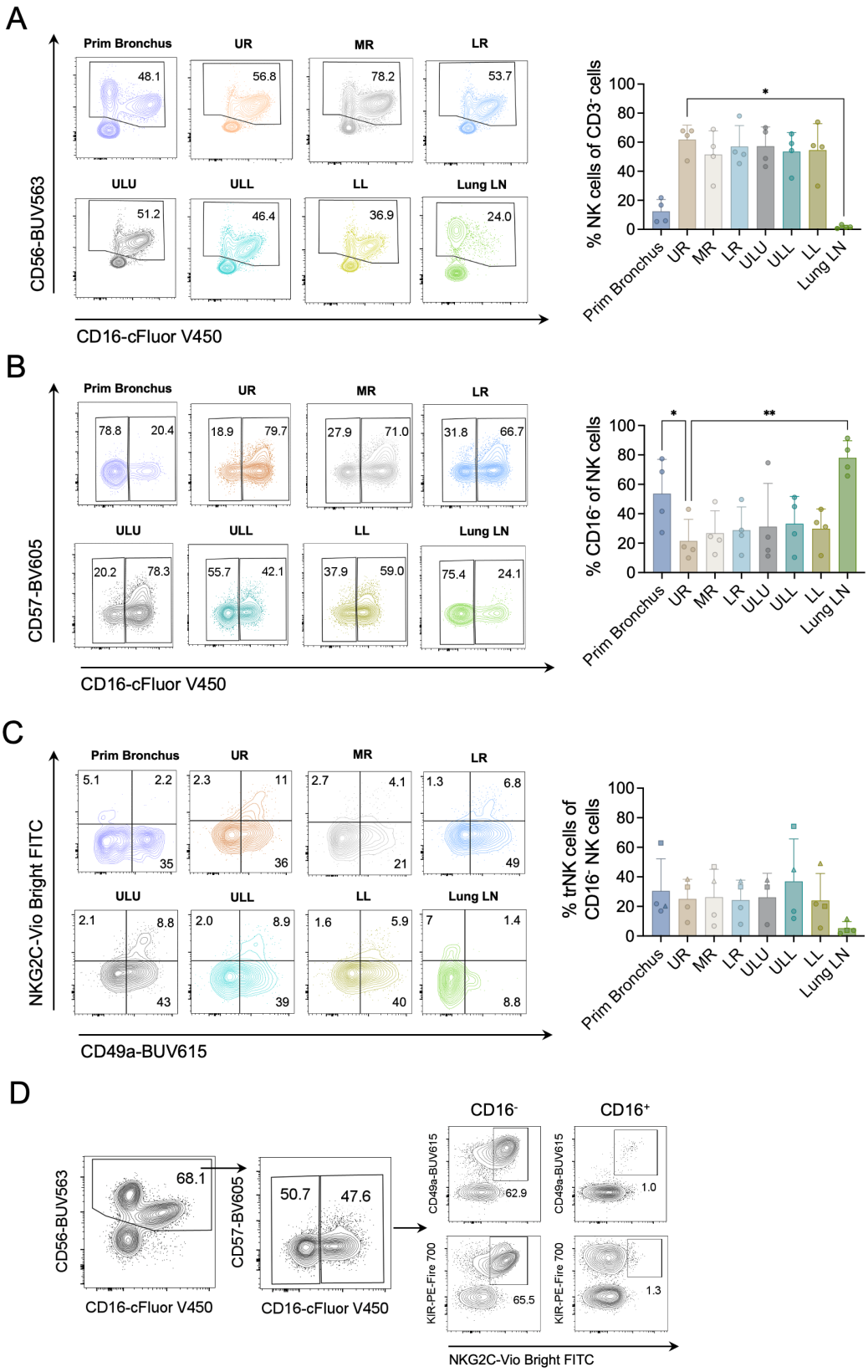

*Figure 6. Identification of NK cells and NK cell subsets in across different lung sections. (A) Representative contour plots (left) and summary of frequencies of NK cells (right) in different lung sections (n=4). (B) Representative contour plots (left) and summary of frequencies of CD16$^-$ NK cells (right) (n=4). (C) Representative contour plots (left) and summary of frequencies of CD16$^-$ trNK cells (right) (n=4). (D) Gating strategy and representative contour plots of CD16$^-$CD49a$^+$ adaptive-like NK cells from donor 1 with expansion. (A-C) Friedman test, Dunn's multiple comparison test (patient-matched), Kruskal-Wallis test (unmatched). *p < 0.05, **p < 0.01, ***p < 0.001, ****p < 0.0001.*

4.3. Interaction between NK cells and human gut tissue using intestinal organoids

In addition to mapping the NK cell landscape in the human lung, this project further focused on establishing a method to study NK cell regulation in the context of human gut tissue immunology. For this purpose, we employed patient-matched intestinal organoids as a model system to investigate the interaction between NK cells and human gut tissue. Ileal and colonic biopsies were obtained from two different patients in order to generate intestinal organoids. A summary of the clinical and demographical details of the patients is displayed in Table 5. The workflow for culturing ileal and colonic organoids depicted in Figure 7. The growth of the organoids was monitored every two days using light microscopy, revealing distinct growth patterns. After eight days of culture, we successfully obtained a sufficient number of ileal and colonic organoids (approximately 180 organoids per two domes). However, already after two to three days, the colonic organoids exhibited significantly faster growth compared to ileal organoids (Figure 8), resulting in substantially larger organoids.

Patient	**n = 2**
Sex	f = 2, m = 0
Mean age (years)	48.5 (min = 37, max = 60)
Reason for colonoscopy	Abdominal pain
Diagnosis	Donor 1: Ileitis Donor 2: No clinical findings

Table 5. Clinical and demographical details of the patients included in the study.

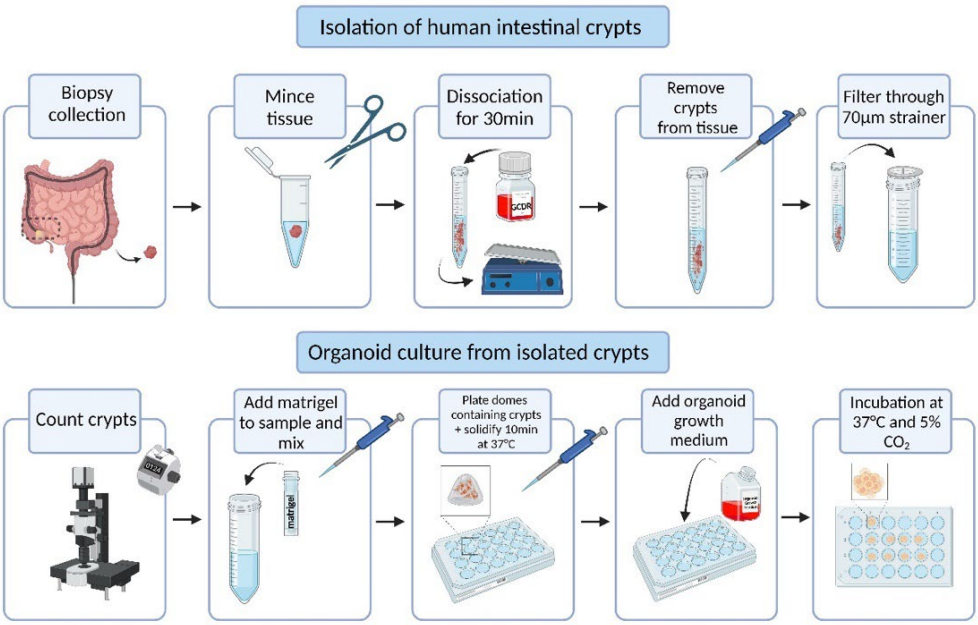

Figure 7. Workflow overview for culturing intestinal organoids from gut biopsies.

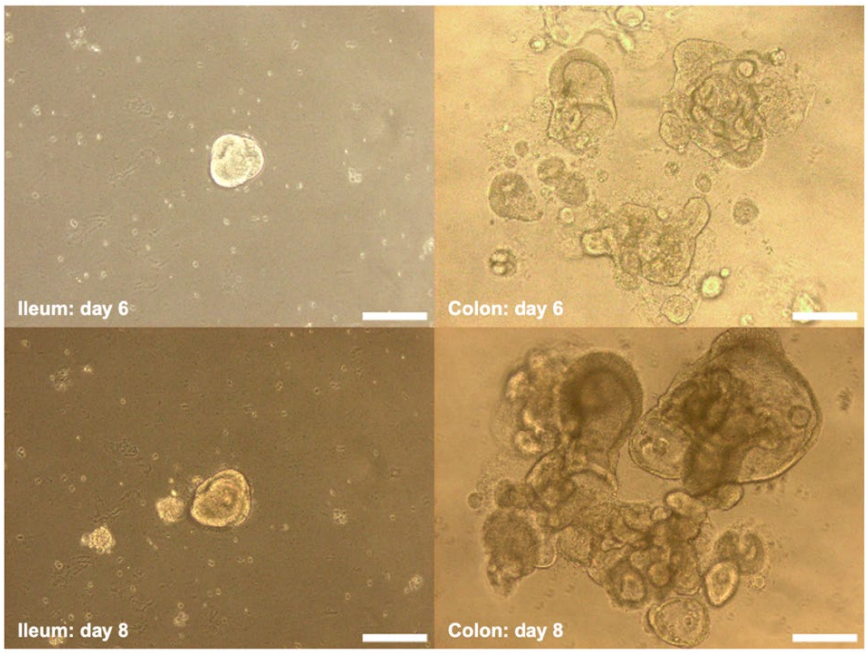

Figure 8. Bright-field microscopy images of ileal and colonic organoids taken on day 6 and day 8 of culture. Scale bar ≙ 200µm.

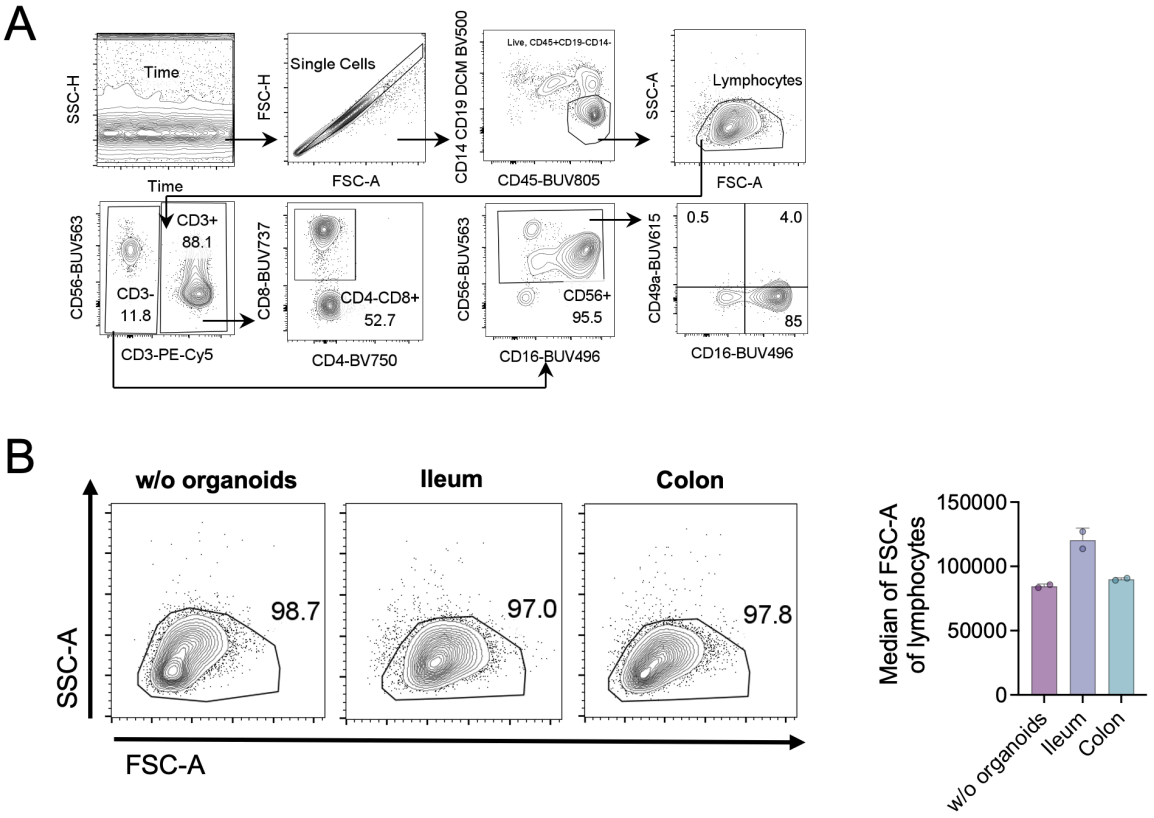

*Figure 9. Flow cytometry analysis of NK cells and CD8⁺ T cells after co-incubation with patient-matched ileal and colonic organoids. (A) Gating strategy for identifying NK cells and CD8⁺ T cells. (B) Representative contour plots (left) and median FSC-A (right) of the lymphocyte populations. Friedman test, Dunn's multiple comparison test (patient-matched). *p < 0.05, **p < 0.01, ***p < 0.001, ****p < 0.0001.*

To assess changes in marker expression and functional characteristics of NK cells and $CD8^+$ T cells upon interaction with ileal and colonic organoids, cryopreserved peripheral blood mononuclear cells (PBMCs) were thawed, stimulated for three hours with 10ng/ml IL-15, and subsequently cultured with or without patient-matched intestinal organoids. Finally, NK and T cell phenotypes were assessed by flow cytometry. Upon identification of NK cells and $CD8^+$ T cells (gating strategy shown in Figure 9A), we observed an increase in the median forward scatter area (FSC-A) of the lymphocyte population upon co-incubation with ileal organoids, compared to both colonic organoids and the control group, indicating an activation of our cells of interest (Figure 9B). Additionally, we confirmed that the NK cells identified in the dataset were derived from blood, as indicated by their high expression of CD16 and their lack of CD49a, suggesting a phenotype of circulating NK cells (Figure 9A).

Further analysis of NK cells and $CD8^+$ T cells following interaction with intestinal organoids from donor 1 revealed that NK cells exhibited slightly lower mean fluorescence intensity (MFI) for GzmA in the respective $GzmA^+$ population, as well as decreased perforin expression after co-incubation with ileal organoids (Figure 10A). Similarly, $CD8^+$ T cells from the same donor showed reduced expression of GzmK and perforin in both colonic and ileal organoids (Figure 10B). Additionally, the MFI of $GzmA^+$ and $GzmB^+$ populations was lower upon co-incubation with intestinal organoids, with a more pronounced decrease observed for GzmA in Ileum. For donor 2, we increased the organoid-to-target cell ratio from 50 organoids:600 000 PBMCs to 180 organoids:750 000 PBMCs by using higher numbers of organoids during co-incubation with patient-matched PBMCs. This adjustment amplified the effects observed in donor 1, which included lower MFI in the GzmA and GzmB in the respective effector molecule-expressing populations of NK cells for both colon and ileum (Figure 11A). We also observed a reduced expression of GzmK and perforin in NK cells, particularly in ileal organoids. $CD8^+$ T cells displayed lower MFIs for $GzmA^+$ and $GzmB^+$ populations after co-incubation with intestinal organoids, again with the most prominent reduction seen with ileal organoids (Figure 11B). Additionally, GzmK expression was reduced in $CD8^+$ T cells upon co-culture with ileal organoids, and perforin was reduced upon co-culture with colonic and ileal organoids. Furthermore, the expression of CD69 was lower in both NK cells and T cells upon co-incubation with intestinal organoids as compared to incubation of PBMCs alone (Figure 11A and B).

In alignment with these results, a quantitative analysis revealed a trend towards reduced expression of effector molecules such as GzmA, GzmB, GzmK, and perforin in both NK cells and T cells following interaction with intestinal organoids, with the most pronounced effects observed in the ileum (Figure 12A and B).

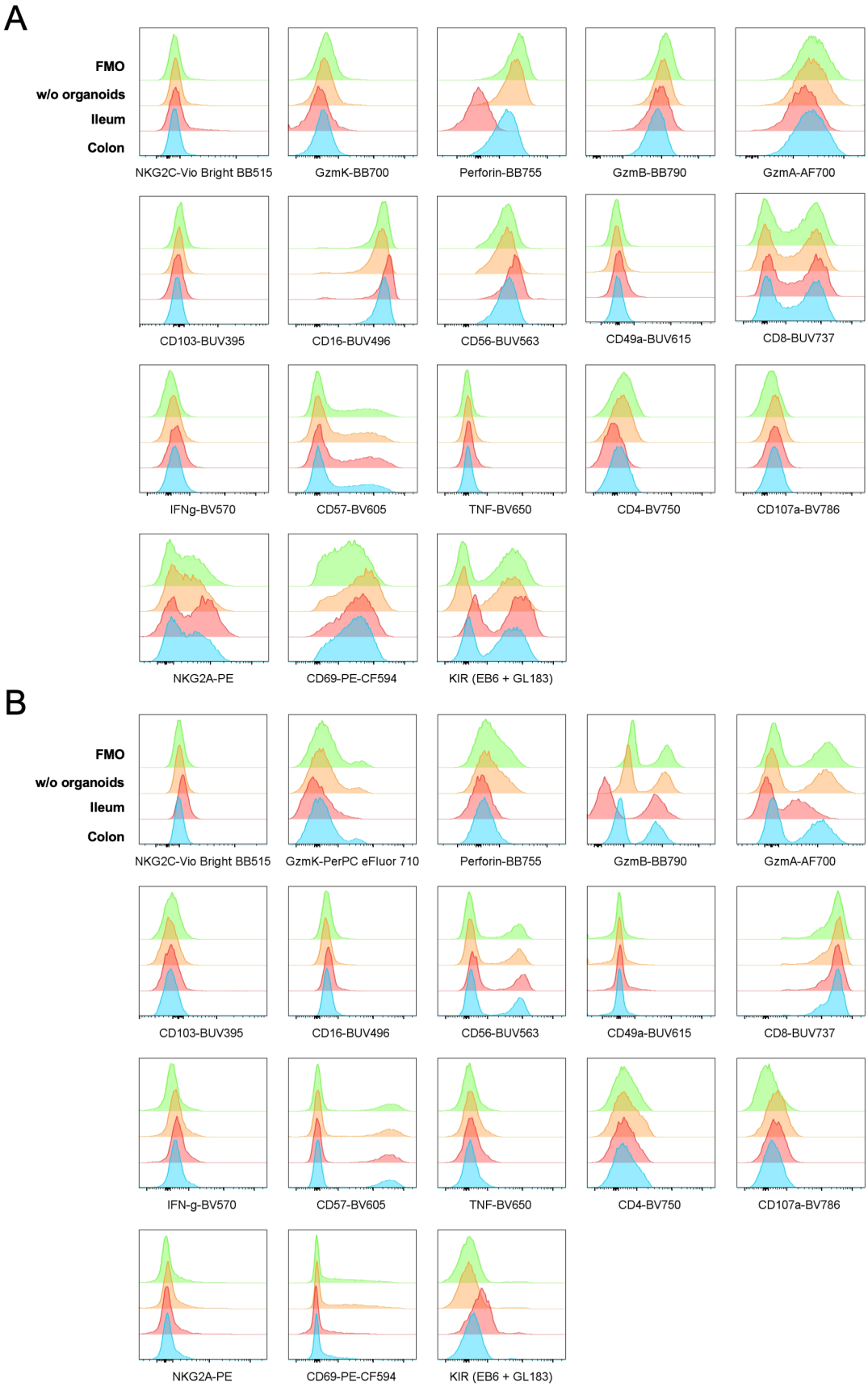

Figure 10. Marker expression of NK cells and CD8⁺ T cells from donor 1 upon co-incubation with patient-matched intestinal organoids. Representative overlays of expression of markers on NK cells (A) and CD8⁺ T cells (B) incubated with ileal organoids (red), colonic organoids (blue) or without organoids (orange). Green histograms represent FMO controls (IFN-γ, TNF, CD107a) incubated without organoids.

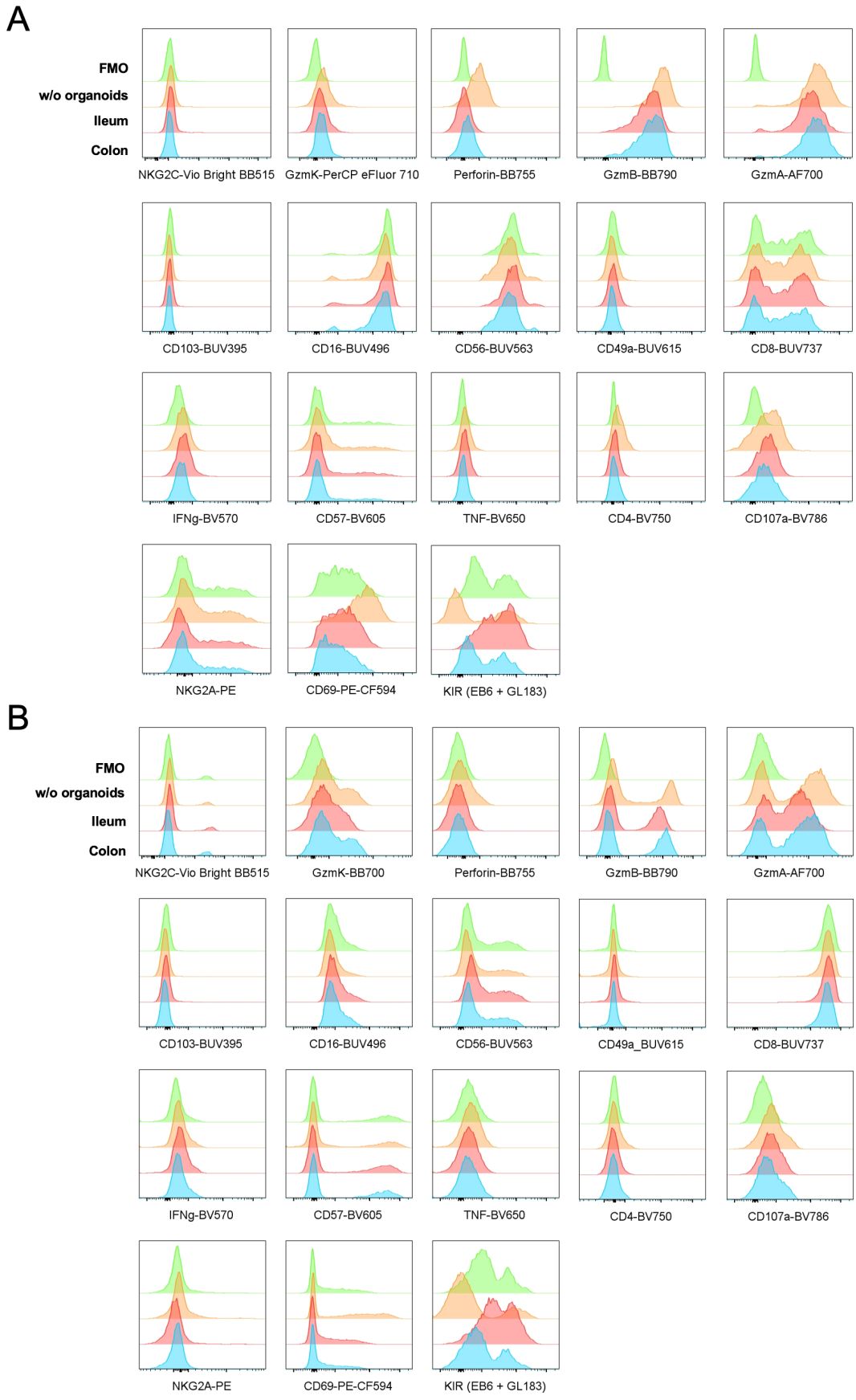

Figure 11. Marker expression of NK cells and CD8⁺ T cells from donor 2 upon co-incubation with patient-matched intestinal organoids. Representative overlays of expression of markers on NK cells (A) and CD8⁺ T cells (B) incubated with ileal organoids (red), colonic organoids (blue) or without organoids (orange). Green histograms represent FMO controls (ICS, CD107a) incubated with colonic organoids.

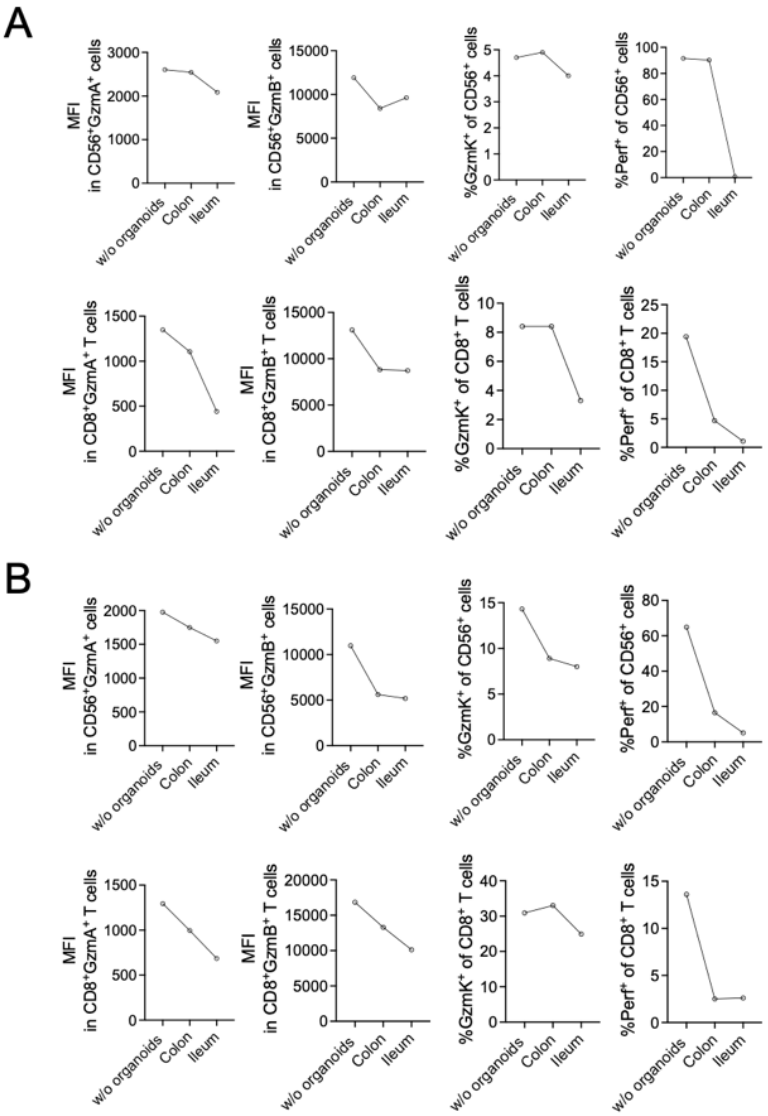

Figure 12. Quantitative analysis of effector molecule expression of NK and CD8⁺ T cells after co-incubation with intestinal organoids. (A) Quantitative analysis of donor 1. (B) Quantitative analysis of donor 2.

5. Discussion

The mucosa of both the respiratory and gastrointestinal tracts is continuously exposed to a wide array of inhaled or ingested antigens, some of which have the potential to cause disease. The bronchus-associated lymphoid tissue (BALT) comprises distinct lymphoid aggregates within the bronchial mucosa. Exhibiting numerous morphological and functional similarities to the GALT, the BALT encompasses a diverse array of immune subsets, exhibiting numerous morphological and functional similarities[163–165]. Mucosal sites within the MALT are thought to communicate via migrating lymphocytes[166,167]. Early studies conducted in mice have verified that influenza-specific T cell clones, when adoptively transferred, exhibit the ability to relocate to the lungs. Furthermore, NK cells have been observed to demonstrate different migratory tendencies towards either the lungs or the gut [168]. In this thesis, to enhance our understanding of the phenotype, distribution, and function of lymphocytes in various human tissues, we aimed to phenotypically define NK cells, and to map their spatial distribution across the human lung. Additionally, we investigated NK cell as well as $CD8^+$ T cell interactions with gut tissues using intestinal organoids as the first and most well-established tissue-derived organoid type.

The human lung mucosa, frequently exposed to foreign antigens, relies on a specialized microenvironment to maintain a balance between tolerance and immune defense. Key to this balance are NK cells, among other lung-resident immune cells[52]. Our comprehensive mapping of the immunological landscape within the human lung revealed distinct distributions of various immune cell subsets across different lung regions. Utilizing spectral flow cytometry, we analyzed viable leukocyte populations from lung donations obtained from four healthy donors.

Our results demonstrated that among all immune cell subsets analyzed, T cells are the most abundant within the MR, surpassing all other leukocyte subsets, including B cells and NK cells, and significantly outnumbering neutrophils and non-NK ILCs. Notably, previous studies have already shown that T cells outnumber B cells by more than 15-fold in the lung[169]. This is in stark contrast to other tissues, such as the spleen, where T and B cells are present at similar frequencies, and in blood and LNs, where T cells outnumber B cells by only 2- to 4-fold or in the ileum and colon, where the ratio of T cells to B cells is 5- to 8-fold[169].

Among T cells, $CD4^+$ T cells were generally more prevalent than $CD8^+$ T cells, suggesting a predominant role for $CD4^+$ T cells in lung immunosurveillance. Detailed analysis of $CD4^+$ T cell subpopulations identified a higher frequency of T_{EM} and T_{CM} compared to T_{EMRA}. In fact, it has been shown previously that $CD4^+$ T cells are the most abundant subset in tissue

sites, with T_{EM} dominating in mucosal tissues such as the lung and T_{CM} accumulating in lymphoid tissues[169]. Conversely, we observed that in the $CD8^+$ T cell subset, T_{EM} and T_{EMRA} cells were predominant, with T_{EM} cells significantly outnumbering naïve T cells. This is consistent with previous findings that show $CD8^+$ T_{EM} cells as the predominant population in mucosal tissues and the spleen, while T_{EMRA} cells accumulate in the blood[169]. Given that the lung is an organ with a substantial blood supply, these findings align well with our observations. Building on these findings, Sathaliyawala *et al*. proposed that $CD8^+$ T cells may actively be stimulated by antigens via the interaction with major histocompatibility complex (MHC) class I-expressing cells within tissues, resulting in their effector differentiation and subsequently in their migration to the peripheral blood[170]. However, a detailed gene expression analysis of $CD4^+$ and $CD8^+$ T cell subsets within tissues would be necessary to fully understand their lineage relationships.

Tregs and γδ T cells were detected at low frequencies within the $CD4^+$ and $CD8^+$ T cell populations, respectively. Comparable frequencies of Tregs have been reported previously, with evidence pointing to the presence of $CD69^+$ tissue-resident Tregs in mucosal sites, including the lung[171]. Analyses within the same study revealed 542 genes differentially expressed between lung Treg and blood Treg subsets, suggesting the presence of a distinct lung-resident Treg subset. Moreover, Tregs are known to suppress effective anti-tumor immune responses in tumor microenvironments. Supporting this, Tregs have been found predominantly in malignant lung tissue areas in NSCLC patients, constituting 25-30% of $CD4^+$ cells, while they were absent in non-malignant lung tissue[172]. γδ T cells are a distinct T cell subpopulation that are known to be present in different peripheral tissues, including the intestines as well as the lungs[173]. By producing substantial amounts of cytokines, γδ T cells play crucial roles in immune responses within these tissues. Notably, one of the infections most strongly associated with γδ T cell responses is CMV, which targets multiple organs, including the intestines, liver, brain, as well as the lungs[173]. Notably, all four investigated donors within our cohort were found to be CMV IgG positive, suggesting a potential influence of the CMV status of the analyzed donors on the observed frequencies of this T cell subset.

Additionally, MAIT cells were present at low frequencies in both $CD4^+$ (0.4%) and $CD8^+$ T cell populations, with a higher prevalence of $CD8^+$ MAIT cells (2-3%). Studies have demonstrated that MAIT cells make up a proportion of 0.37–4.90% of all $CD3^+$ T cells in the human lung[174]. However, using a different gating strategy where MAIT cells were identified as $CD3^+$ MR1/5-OP-RU^+ and then analyzed for expression of CD8 and CD4, approximately half of the MAIT cells in the lung did not express high levels of the co-receptors CD8 or CD4, in contrast to MAIT cells from PBMCs[174], suggesting that MAIT frequencies in the investigated lungs might in fact be higher than observed. Playing a

crucial role in respiratory bacterial infections due to their effective responses to bacteria-infected cells, MAIT cells were shown to be particularly abundant in the human airways[175,176].

Since our study was focussing on lymphocytes, particularly NK cells and $CD8^+$ T cells, and their tissue-resident subsets, we analyzed T_{RM} cells across four lung regions, including the primary bronchus as well as three parenchyma sites in the right lung lobe (UR, MR, and LR). Significant differences were found in the $CD4^+$ T_{RM} population, with higher frequencies in the LR compared to the primary bronchus. Although $CD8^+$ T_{RM} frequencies decreased from the primary bronchus down to the LR, this trend was not statistically significant. These findings indicate regional variations in T_{RM} frequencies within the human lung. It is known that in the human lung, $CD4^+$ and $CD8^+$ T lymphocytes serve as the primary adaptive immune cells, with non-circulating T_{RM} cells comprising the major T cell subset of those T cells[177–179]. Previous studies on human lung T_{RM} have shown that T_{RM} are distributed throughout various regions of the respiratory tract, including the parenchyma, airways, and associated lymph nodes, indicating their involvement in protection, immunosurveillance, and homeostasis[179–182]. Moreover, immunohistochemistry analyses of non-diseased human lung sections revealed that T cells in adult lungs are accumulated near the airways[183]. However, Synder *et al.* conclude that a more detailed spatial analysis is required to comprehensively understand the organization of T_{RM} within the complex lung structures. In this study, we give an overview of the spatial distribution of $CD4^+$ and $CD8^+$ T_{RM} cells across eight different anatomical regions, including the primary bronchus, six different parenchyma sites within the left and the right lung lobe as well as lung-associated LNs.

Our analysis of B cells showed very low frequencies of plasma cells as well as IgD^+ B cells being more prevalent. Previously healthy individuals were found to continuously contain low but detectable frequencies of plasmablasts in blood and, as indicated by the expression of IgA, CCR10, $\alpha4\beta7$ integrin as well as the secretion of polymeric IgA, most of these plasmablasts seem to be generated in the course of mucosal immune reactions in the gut and/or the airways[184–187]. Moreover, lung-resident memory B cells were shown to play a crucial role in the immunity to respiratory viruses like influenza virus[188]. The expression of IgD appears to be vital for immune surveillance, strategically positioned at mucosal sites like the nasopharyngeal cavities where antigens enter[189]. It establishes a mutualistic interaction with the commensal microbiota, thus regulating mucosal homeostasis. Additionally, the secretion of IgD equips basophils and mast cells with IgD antibodies, enabling them to respond to both commensal and pathogenic microbes[189]. Overall, these findings confirm our observations of the presence of B cells within the

investigated lung tissues with low frequencies of plasmablasts as well as the relatively high abundancy of IgD^+ B cells.

In addition to the above-described immune subsets, we also identified ILCs of type 1, 2, and 3, with ILC1/2s comprising the predominant subset. These results align with the findings of studies that have characterized these subsets in the human lung before[190]. Observed in different tissues such as intestines and, less defined, the lung, ILCs are a recently defined but important component of the innate immune system, with knowledge limited to ILC2s[67,190,191].

As a part of the group 1 ILCs, we were particularly interested in the phenotype as well as the spatial distribution of NK cells across different human lung areas and associated tissues. A detailed analysis of NK cells across eight distinct anatomical regions of the lung including the primary bronchus, six parenchymal sites as well as lung LNs revealed that NK cells were present in all regions, with the highest frequencies observed in lung parenchyma sections (52-62% of $CD3^-$ cells). Lower frequencies were noted in the primary bronchus and lung LNs. As previously described in the literature, NK cells are most abundant in lung, blood, bone marrow and spleen and less prominent in LNs, tonsils, and intestines, which is in accordance with our findings[30]. Further quantification of $CD16^-$ and $CD16^+$ NK cell subsets indicated higher frequencies of $CD16^-$ NK cells in the lung LN and primary bronchus, with lower frequencies in parenchymal sites. Due to the high vascularization of the lung, the predominance of $CD16^+$ NK cells in parenchymal sites was expected. These $CD16^+$ NK cells represent a mature and terminally differentiated NK cell subset[30,192]. Conversely, less mature subsets, characterized by the lack of CD16 and diminished effector capacity, are localized in the LNs and primary bronchus. This distribution pattern is supported by a previous study, in which the distribution of NK cells across different human organs obtained from organ donors was analyzed[30]. Similarly to our results, Dogra *et al.* identified terminally differentiated NK cells in blood and blood-rich organs such as the lung whereas the immature $CD16^-$ NK cells were described as predominant in LNs, tonsils as well as the GI tract[30].

As it is characteristic for trNK cells to be less differentiated and to lack the expression of CD16[52], frequencies of trNK cells, identified by CD69, CD49a, and/or CD103 expression, were investigated within the $CD16^-$ NK cell population. Comparative analysis showed trNK cell frequencies between 24% and 37% across all lung regions, whereas lung LN exhibited lower frequencies (5%). Notably, two donors exhibited high frequencies of $CD16^-CD49a^+$ adaptive-like trNK cells and appeared to be outnumbering the $CD16^+CD57^+NKG2C^+$ adaptive-like NK cell subset known to be present in in the human blood and in blood-rich organs[30,61,62]. This $CD16^-CD49a^+$ adaptive-like trNK cell subset with high effector function and tissue-residency features has earlier been described by our group within the human

lung[60]. Together, our results provide insights into lung tissue site-driven segregation of NK cell subsets and development and are in accordance with findings that have previously been made.

Representing vital components of the innate immune system, NK cells and ILCs serve as the first line of defense against pathogenic microorganisms in the gut[7,33,66]. Distributed throughout the epithelium and stroma, gut NK cells interact with various cell types to maintain immune homeostasis, respond to infections, and regulate immune responses by producing IFN-γ[64,67]. Their involvement extends to IBD such as CD and UC, which heighten the risk of CRC[68–70]. In this thesis, in order to explore the interaction between human NK cells and gut tissue, we utilized patient-matched intestinal organoids as model systems. Upon co-incubation of patient-matched PBMCs with ileal organoids, the data suggest minor activation of NK cells and $CD8^+$ T cells, as indicated by a higher median of the FSC-A of lymphocytes, corresponding to increased cell size after coculture with organoids derived from the ileum but not the colon. Effector molecule expression was decreased upon coculture with organoids, particularly in NK cells and $CD8^+$ T cells incubated with ileal organoids, indicating that gut tissue might modulate immune cell activity. Granzymes are serine proteases predominantly produced by cytotoxic lymphocytes such as NK cells and $CD8^+$ T cells. They are traditionally considered to cause apoptosis in tumor cells and virally infected cells. However, they have been described to also regulate proinflammatory cytokine responses[193]. Studies in the context of CD revealed that GzmB secreted by $CD8^+$ T cells acted on other $CD8^+$ T cells, potentially inducing the release of proinflammatory cytokines and therefore suggesting a mechanism of granzymes promoting inflammation in IBD[194]. In fact, GzmA was previously shown to stimulate the release of proinflammatory cytokines in human monocytic cells[195]. Further studies reported that GzmK-expressing $CD8^+$ T cells are also the predominant $CD8^+$ T cell population in the gut and other tissues, suggesting that these cells constitute a core population of tissue-associated T cells across various human tissues[196]. In mice, depleting NK cells and ablating perforin (but not granulocytes or T cells) led to delayed tissue inflammation following infection with *Salmonella* Typhimurium[197]. This indicates that the perforin response of NK cells is a crucial factor in initiating gut mucosal inflammation. Further, perforin has also been shown to play a role in controlling the expansion and elimination of activated $CD8^+$ T cells during chronic and after viral infections, suggesting that targeting the production of cytolytic molecules could offer therapeutic benefits for IBD[194,198,199]. In our study, exposure to intestinal organoids resulted in decreased granzyme and perforin expression in NK and $CD8^+$ T cells, suggesting that gut tissue might modulate immune responses, potentially leading to an increased release of effector molecules. However, further investigations are necessary to confirm this hypothesis. Noteworthy to mention here is that donor 2 was

diagnosed with acute Ileitis, which might potentially influence the phenotypes observed within this study.

Since our results did not yet reach statistical significance, further investigation involving a larger number of patients is necessary. Moreover, given the limited number of studies analyzing the interaction between NK cells and intestinal organoids[123], our protocol may require further optimization. Extending the duration of PBMC stimulation and coculture with patient-matched organoids, for example, may enhance observed effects and better replicate physiological conditions, particularly in the context of ongoing stress such as infections. Limitations were encountered due to constraints in the number of organoids and PBMCs and therefore in selecting specific PBMC:organoid ratios as well as harvesting sufficient PBMCs for flow cytometry analysis. Future investigations could involve organoids derived from patients with IBD to explore the phenotypic characteristics of NK and T cells upon interaction. Together, these findings underscore the influence of the gut microenvironment on the phenotypic characteristics of NK and $CD8^+$ T cells, suggesting a role for tissue-specific interactions in modulating systemic immune responses.

Overall, our study provides a detailed characterization of the immune cell landscape within the human lung, highlighting the predominance of T cells and significant regional variations in immune cell distributions. Additionally, the presence of diverse NK cell subsets across lung regions and the modulation of immune cell phenotypes by gut tissue interactions offer valuable insights into the complexity of immune regulation in different tissue environments. These findings contribute to our understanding of tissue-specific immune responses and may help in improving or developing therapeutic strategies for respiratory and gastrointestinal diseases, such as lung cancer and IBD.

6. References

1. Kiessling, R., Klein, E. & Wigzell, H. „Natural" killer cells in the mouse. I. Cytotoxic cells with specificity for mouse Moloney leukemia cells. Specificity and distribution according to genotype. *Eur J Immunol* **5**, (1975).
2. Herberman, R. B., Nunn, M. E., Holden, H. T. & Lavrin, D. H. Natural cytotoxic reactivity of mouse lymphoid cells against syngeneic and allogeneic tumors. II. Characterization of effector cells. *Int J Cancer* **16**, (1975).
3. Myers, J. A. & Miller, J. S. Exploring the NK cell platform for cancer immunotherapy. *Nature Reviews Clinical Oncology* vol. 18 Preprint at https://doi.org/10.1038/s41571-020-0426-7 (2021).
4. Cella, M. *et al.* A human natural killer cell subset provides an innate source of IL-22 for mucosal immunity. *Nature* **457**, (2009).
5. Diefenbach, A., Colonna, M. & Koyasu, S. Development, differentiation, and diversity of innate lymphoid cells. *Immunity* vol. 41 Preprint at https://doi.org/10.1016/j.immuni.2014.09.005 (2014).
6. Colonna, M. Innate Lymphoid Cells: Diversity, Plasticity, and Unique Functions in Immunity. *Immunity* vol. 48 Preprint at https://doi.org/10.1016/j.immuni.2018.05.013 (2018).
7. Spits, H., Bernink, J. H. & Lanier, L. NK cells and type 1 innate lymphoid cells: Partners in host defense. *Nature Immunology* vol. 17 Preprint at https://doi.org/10.1038/ni.3482 (2016).
8. Mace, E. M. Human natural killer cells: Form, function, and development. *Journal of Allergy and Clinical Immunology* **151**, (2023).
9. Bryceson, Y. T., March, M. E., Ljunggren, H. G. & Long, E. O. Activation, coactivation, and costimulation of resting human natural killer cells. *Immunological Reviews* vol. 214 Preprint at https://doi.org/10.1111/j.1600-065X.2006.00457.x (2006).
10. Bryceson, Y. T. *et al.* Molecular mechanisms of natural killer cell activation. *Journal of Innate Immunity* vol. 3 Preprint at https://doi.org/10.1159/000325265 (2011).
11. Long, E. O. Negative signaling by inhibitory receptors: The NK cell paradigm. *Immunological Reviews* vol. 224 Preprint at https://doi.org/10.1111/j.1600-065X.2008.00660.x (2008).

12. Parham, P., Norman, P. J., Abi-Rached, L. & Guethlein, L. A. Human-specific evolution of killer cell immunoglobulin-like receptor recognition of major histocompatibility complex class I molecules. *Philosophical Transactions of the Royal Society B: Biological Sciences* vol. 367 Preprint at https://doi.org/10.1098/rstb.2011.0266 (2012).
13. Quatrini, L. *et al.* The immune checkpoint PD-1 in natural killer cells: Expression, function and targeting in tumour immunotherapy. *Cancers* vol. 12 Preprint at https://doi.org/10.3390/cancers12113285 (2020).
14. Stanietsky, N. *et al.* The interaction of TIGIT with PVR and PVRL2 inhibits human NK cell cytotoxicity. *Proc Natl Acad Sci U S A* **106**, (2009).
15. Ndhlovu, L. C. *et al.* Tim-3 marks human natural killer cell maturation and suppresses cell-mediated cytotoxicity. in *Blood* vol. 119 (2012).
16. Kärre, K., Ljunggren, H. G., Piontek, G. & Kiessling, R. Selective rejection of H-2-deficient lymphoma variants suggests alternative immune defence strategy. *Nature* **319**, (1986).
17. Ljunggren, H. G. & Kärre, K. In search of the 'missing self': MHC molecules and NK cell recognition. *Immunol Today* **11**, (1990).
18. Barrow, A. D., Martin, C. J. & Colonna, M. The natural cytotoxicity receptors in health and disease. *Frontiers in Immunology* vol. 10 Preprint at https://doi.org/10.3389/fimmu.2019.00909 (2019).
19. Zingoni, A. *et al.* NKG2D and its ligands: 'One for all, all for one'. *Frontiers in Immunology* vol. 9 Preprint at https://doi.org/10.3389/fimmu.2018.00476 (2018).
20. Schlums, H. *et al.* Cytomegalovirus infection drives adaptive epigenetic diversification of NK cells with altered signaling and effector function. *Immunity* **42**, (2015).
21. Fauriat, C., Long, E. O., Ljunggren, H. G. & Bryceson, Y. T. Regulation of human NK-cell cytokine and chemokine production by target cell recognition. *Blood* **115**, (2010).
22. Cooper, M. A., Fehniger, T. A. & Caligiuri, M. A. The biology of human natural killer-cell subsets. *Trends in Immunology* vol. 22 Preprint at https://doi.org/10.1016/S1471-4906(01)02060-9 (2001).

23. Björkström, N. K., Ljunggren, H. G. & Michaëlsson, J. Emerging insights into natural killer cells in human peripheral tissues. *Nature Reviews Immunology* vol. 16 Preprint at https://doi.org/10.1038/nri.2016.34 (2016).
24. Robertson, M. J. & Ritz, J. Biology and clinical relevance of human natural killer cells. *Blood* vol. 76 Preprint at https://doi.org/10.1182/blood.v76.12.2421.bloodjournal76122421 (1990).
25. Björkström, N. K. *et al.* Expression patterns of NKG2A, KIR, and CD57 define a process of CD56 dim NK-cell differentiation uncoupled from NK-cell education. *Blood* **116**, (2010).
26. Lopez-Vergès, S. *et al.* CD57 defines a functionally distinct population of mature NK cells in the human CD56dimCD16+ NK-cell subset. *Blood* **116**, (2010).
27. Cooper, M. A. *et al.* Human natural killer cells: A unique innate immunoregulatory role for the CD56bright subset. *Blood* **97**, (2001).
28. Lanier, L. L., Le, A. M., Civin, C. I., Loken, M. R. & Phillips, J. H. The relationship of CD16 (Leu-11) and Leu-19 (NKH-1) antigen expression on human peripheral blood NK cells and cytotoxic T lymphocytes. *The Journal of Immunology* **136**, (1986).
29. Prager, I. *et al.* NK cells switch from granzyme B to death receptor-mediated cytotoxicity during serial killing. *Journal of Experimental Medicine* **216**, (2019).
30. Dogra, P. *et al.* Tissue Determinants of Human NK Cell Development, Function, and Residence. *Cell* **180**, (2020).
31. Fehniger, T. A. *et al.* CD56bright natural killer cells are present in human lymph nodes and are activated by T cell-derived IL-2: A potential new link between adaptive and innate immunity. *Blood* **101**, (2003).
32. Hudspeth, K. *et al.* Human liver-resident CD56bright/CD16neg NK cells are retained within hepatic sinusoids via the engagement of CCR5 and CXCR6 pathways. *J Autoimmun* **66**, (2016).
33. Sagebiel, A. F. *et al.* Tissue-resident Eomes + NK cells are the major innate lymphoid cell population in human infant intestine. *Nat Commun* **10**, (2019).
34. Montaldo, E. *et al.* Unique Eomes+ NK cell subsets are present in uterus and decidua during early pregnancy. *Front Immunol* **6**, (2016).

35. Peng, H. *et al.* Liver-resident NK cells confer adaptive immunity in skin-contact inflammation. *Journal of Clinical Investigation* **123**, (2013).
36. Marquardt, N. *et al.* Human lung natural killer cells are predominantly comprised of highly differentiated hypofunctional CD69−CD56dim cells. *Journal of Allergy and Clinical Immunology* **139**, (2017).
37. Scheffschick, A. *et al.* Skin infiltrating NK cells in cutaneous T-cell lymphoma are increased in number and display phenotypic alterations partially driven by the tumor. *Front Immunol* **14**, (2023).
38. Sojka, D. K. *et al.* Tissue-resident natural killer (NK) cells are cell lineages distinct from thymic and conventional splenic NK cells. *Elife* **2014**, (2014).
39. Peng, H. & Tian, Z. Diversity of tissue-resident NK cells. *Seminars in Immunology* vol. 31 Preprint at https://doi.org/10.1016/j.smim.2017.07.006 (2017).
40. Shiow, L. R. *et al.* CD69 acts downstream of interferon-α/β to inhibit S1P 1 and lymphocyte egress from lymphoid organs. *Nature* **440**, (2006).
41. Speak, A. O. *et al.* Altered distribution and function of natural killer cells in murine and human Niemann-Pick disease type C1. *Blood* **123**, (2014).
42. Ottaviani, C. *et al.* CD56brightCD16- NK cells accumulate in psoriatic skin in response to CXCL10 and CCL5 and exacerbate skin inflammation. *Eur J Immunol* **36**, (2006).
43. Marquardt, N. *et al.* Cutting Edge: Identification and Characterization of Human Intrahepatic CD49a+ NK Cells. *The Journal of Immunology* **194**, (2015).
44. Burt, B. M. *et al.* The Lytic Potential of Human Liver NK Cells Is Restricted by Their Limited Expression of Inhibitory Killer Ig-Like Receptors. *The Journal of Immunology* **183**, (2009).
45. Ali, T. H. *et al.* Enrichment of CD56dimKIR+CD57+ highly cytotoxic NK cells in tumour-infiltrated lymph nodes of melanoma patients. *Nat Commun* **5**, (2014).
46. Hemler, M. E. VLA proteins in the integrin family: Structures, functions, and their role on leukocytes. *Annu Rev Immunol* **8**, (1990).
47. Khalilgharibi, N. & Mao, Y. To form and function: On the role of basement membrane mechanics in tissue development, homeostasis and disease. *Open Biology* vol. 11 Preprint at https://doi.org/10.1098/rsob.200360 (2021).

48. Fuchs, A. *et al.* Intraepithelial type 1 innate lymphoid cells are a unique subset of il-12- and il-15-responsive ifn-γ-producing cells. *Immunity* **38**, (2013).
49. Hadley, G. A. & Higgins, J. M. G. Integrin αeβ7: Molecular features and functional significance in the immune system. *Adv Exp Med Biol* **819**, (2014).
50. Cepek, K. L. *et al.* Adhesion between epithelial cells and T lymphocytes mediated by E-cadherin and the αeβ7 integrin. *Nature* **372**, (1994).
51. Cortez, V. S., Fuchs, A., Cella, M., Gilfillan, S. & Colonna, M. Cutting Edge: Salivary Gland NK Cells Develop Independently of Nfil3 in Steady-State. *The Journal of Immunology* **192**, (2014).
52. Marquardt, N. *et al.* Unique transcriptional and protein-expression signature in human lung tissue-resident NK cells. *Nat Commun* **10**, (2019).
53. Ardain, A., Marakalala, M. J. & Leslie, A. Tissue-resident innate immunity in the lung. *Immunology* vol. 159 Preprint at https://doi.org/10.1111/imm.13143 (2020).
54. Hewitt, R. J. & Lloyd, C. M. Regulation of immune responses by the airway epithelial cell landscape. *Nature Reviews Immunology* vol. 21 Preprint at https://doi.org/10.1038/s41577-020-00477-9 (2021).
55. Tomasello, E. *et al.* Mapping of NKp46+ cells in healthy human lymphoid and non-lymphoid tissues. *Front Immunol* **3**, (2012).
56. Cooper, G. E., Ostridge, K., Khakoo, S. I., Wilkinson, T. M. A. & Staples, K. J. Human CD49a+ lung natural killer cell cytotoxicity in response to influenza A virus. *Front Immunol* **9**, (2018).
57. Yamamoto, Y. *et al.* Lung-resident natural killer cells control pulmonary tumor growth in mice. *Cancer Sci* **109**, (2018).
58. Jegaskanda, S., Weinfurter, J. T., Friedrich, T. C. & Kent, S. J. Antibody-Dependent Cellular Cytotoxicity Is Associated with Control of Pandemic H1N1 Influenza Virus Infection of Macaques. *J Virol* **87**, (2013).
59. Wang, J. *et al.* Lung natural killer cells in mice: Phenotype and response to respiratory infection. *Immunology* **137**, (2012).
60. Brownlie, D. *et al.* Expansions of adaptive-like NK cells with a tissue-resident phenotype in human lung and blood. *Proc Natl Acad Sci U S A* **118**, (2021).
61. Sun, J. C., Beilke, J. N. & Lanier, L. L. Adaptive immune features of natural killer cells. *Nature* **457**, (2009).

62. Haroun-Izquierdo, A. *et al.* Adaptive single-KIR + NKG2C + NK cells expanded from select superdonors show potent missing-self reactivity and efficiently control HLA-mismatched acute myeloid leukemia. *J Immunother Cancer* **10**, (2022).
63. Gumá, M. *et al.* Imprint of human cytomegalovirus infection on the NK cell receptor repertoire. *Blood* **104**, (2004).
64. Poggi, A. *et al.* Human gut-associated natural killer cells in health and disease. *Frontiers in Immunology* vol. 10 Preprint at https://doi.org/10.3389/fimmu.2019.00961 (2019).
65. Kayama, H., Okumura, R. & Takeda, K. Interaction between the Microbiota, Epithelia, and Immune Cells in the Intestine. *Annu Rev Immunol* **38**, (2020).
66. Spits, H. & Di Santo, J. P. The expanding family of innate lymphoid cells: Regulators and effectors of immunity and tissue remodeling. *Nature Immunology* vol. 12 Preprint at https://doi.org/10.1038/ni.1962 (2011).
67. Spits, H. *et al.* Innate lymphoid cells-a proposal for uniform nomenclature. *Nat Rev Immunol* **13**, (2013).
68. Ekbom, A., Helmick, C., Zack, M. & Adami, H. O. Ulcerative colitis and colorectal cancer. A population-based study. *N Engl J Med* **323**, (1990).
69. Mattar, M. C., Lough, D., Pishvaian, M. J. & Charabaty, A. Current management of inflammatory bowel disease and colorectal cancer. *Gastrointestinal Cancer Research* vol. 4 Preprint at (2011).
70. Buonocore, S. *et al.* Innate lymphoid cells drive interleukin-23-dependent innate intestinal pathology. *Nature* **464**, (2010).
71. Berahovich, R. D., Lai, N. L., Wei, Z., Lanier, L. L. & Schall, T. J. Evidence for NK Cell Subsets Based on Chemokine Receptor Expression. *The Journal of Immunology* **177**, (2006).
72. Campbell, J. J. *et al.* Unique Subpopulations of CD56+ NK and NK-T Peripheral Blood Lymphocytes Identified by Chemokine Receptor Expression Repertoire. *The Journal of Immunology* **166**, (2001).
73. Lima, M. *et al.* Chemokine Receptor Expression on Normal Blood CD56+ NK-Cells Elucidates Cell Partners That Comigrate during the Innate and Adaptive Immune Responses and Identifies a Transitional NK-Cell Population. *J Immunol Res* **2015**, (2015).

74. Lanier, L. L., Chang, C. & Phillips, J. H. Human NKR-P1A. A disulfide-linked homodimer of the C-type lectin superfamily expressed by a subset of NK and T lymphocytes. *The Journal of Immunology* **153**, (1994).
75. Poggi, A. *et al.* Expression of human NKRP1A by CD34+ immature thymocytes: NKRP1A-mediated regulation of proliferation and cytolytic activity. *Eur J Immunol* **26**, (1996).
76. Llibre, A. *et al.* Expression of lectin-like transcript-1 in human tissues. *F1000Res* **5**, (2016).
77. Bernink, J. H. *et al.* Human type 1 innate lymphoid cells accumulate in inflamed mucosal tissues. *Nat Immunol* **14**, (2013).
78. Poggi, A., Costa, P., Zocchi, M. R. & Moretta, L. Phenotypic and functional analysis of CD4+ NKRP1A+ human T lymphocytes. Direct evidence that the NKRP1A molecule is involved in transendothelial migration. *Eur J Immunol* **27**, (1997).
79. Hanna, J. *et al.* CXCL12 expression by invasive trophoblasts induces the specific migration of CD16- human natural killer cells. *Blood* **102**, (2003).
80. Bernardini, G. *et al.* CCL3 and CXCL12 regulate trafficking of mouse bone marrow NK cell subsets. *Blood* **111**, (2008).
81. Leiter, A., Veluswamy, R. R. & Wisnivesky, J. P. The global burden of lung cancer: current status and future trends. *Nature Reviews Clinical Oncology* vol. 20 Preprint at https://doi.org/10.1038/s41571-023-00798-3 (2023).
82. Travis, W. D. *et al.* WHO Classification of Tumours of the Lung, Pleura, Thymus and Heart. *J Thorac Oncol* **10**, (2015).
83. Schabath, M. B. & Cote, M. L. Cancer progress and priorities: Lung cancer. *Cancer Epidemiology Biomarkers and Prevention* **28**, (2019).
84. Imai, K., Matsuyama, S., Miyake, S., Suga, K. & Nakachi, K. Natural cytotoxic activity of peripheral-blood lymphocytes and cancer incidence: An 11-year follow-up study of a general population. *Lancet* **356**, (2000).
85. López-Soto, A., Gonzalez, S., Smyth, M. J. & Galluzzi, L. Control of Metastasis by NK Cells. *Cancer Cell* vol. 32 Preprint at https://doi.org/10.1016/j.ccell.2017.06.009 (2017).
86. Carrega, P. *et al.* Natural killer cells infiltrating human nonsmall-cell lung cancer are enriched in CD56brightCD16- cells and display an impaired capability to kill tumor cells. *Cancer* **112**, (2008).

87. Loeffler, D. A., Heppner, G. H. & Juneau, P. L. Natural killer-cell activity under conditions reflective of tumor micro-environment. *Int J Cancer* **48**, (1991).
88. Hasegawa, Y. *et al.* Transforming growth factor-β1 level correlates with angiogenesis, tumor progression, and prognosis in patients with nonsmall cell lung carcinoma. *Cancer* **91**, (2001).
89. Chen, X. *et al.* Tissue-resident CD69+CXCR6+ Natural Killer cells with exhausted phenotype accumulate in human non-small cell lung cancer. *Eur J Immunol* **52**, (2022).
90. Iuliano, A. D. *et al.* Estimates of global seasonal influenza-associated respiratory mortality: a modelling study. *The Lancet* **391**, (2018).
91. Björkström, N. K., Strunz, B. & Ljunggren, H. G. Natural killer cells in antiviral immunity. *Nature Reviews Immunology* vol. 22 Preprint at https://doi.org/10.1038/s41577-021-00558-3 (2022).
92. Mandelboim, O. *et al.* Recognition of haemagglutinins on virus-infected cells by NKp46 activates lysis by human NK cells. *Nature* **409**, (2001).
93. Draghi, M. *et al.* NKp46 and NKG2D Recognition of Infected Dendritic Cells Is Necessary for NK Cell Activation in the Human Response to Influenza Infection. *The Journal of Immunology* **178**, (2007).
94. Scharenberg, M. *et al.* Influenza A virus infection induces hyperresponsiveness in human lung tissue-resident and peripheral blood NK cells. *Front Immunol* **10**, (2019).
95. Xu, G. *et al.* The differential immune responses to COVID-19 in peripheral and lung revealed by single-cell RNA sequencing. *Cell Discov* **6**, (2020).
96. Maucourant, C. *et al.* Natural killer cell immunotypes related to COVID-19 disease severity. *Sci Immunol* **5**, (2020).
97. Lee, M. J. & Blish, C. A. Defining the role of natural killer cells in COVID-19. *Nature Immunology* vol. 24 Preprint at https://doi.org/10.1038/s41590-023-01560-8 (2023).
98. Baumgart, D. C. & Carding, S. R. Inflammatory bowel disease: cause and immunobiology. *Lancet* vol. 369 Preprint at https://doi.org/10.1016/S0140-6736(07)60750-8 (2007).
99. Geremia, A. & Arancibia-Cárcamo, C. V. Innate lymphoid cells in intestinal inflammation. *Frontiers in Immunology* vol. 8 Preprint at https://doi.org/10.3389/fimmu.2017.01296 (2017).

100. Fathollahi, A., Aslani, S., Mostafaei, S., Rezaei, N. & Mahmoudi, M. The role of killer-cell immunoglobulin-like receptor (KIR) genes in susceptibility to inflammatory bowel disease: systematic review and meta-analysis. *Inflammation Research* vol. 67 Preprint at https://doi.org/10.1007/s00011-018-1162-7 (2018).
101. Wang, F. *et al.* Regulatory role of NKG2D+ NK cells in intestinal lamina propria by secreting double-edged Th1 cytokines in ulcerative colitis. *Oncotarget* **8**, (2017).
102. Takayama, T. *et al.* Imbalance of NKp44+NKp46- and NKp44 -NKp46+ natural killer cells in the intestinal mucosa of patients with Crohn's disease. *Gastroenterology* **139**, (2010).
103. Bauer, S. *et al.* Activation of NK cells and T cells by NKG2D, a receptor for stress- inducible MICA. *Science (1979)* **285**, (1999).
104. Perera, L. *et al.* Expression of nonclassical class I molecules by intestinal epithelial cells. *Inflamm Bowel Dis* **13**, (2007).
105. Scherer, W. F., Syverton, J. T. & Gey, G. O. Studies on the propagation in vitro of poliomyelitis viruses: IV. Viral multiplication in a stable strain of human malignant epithelial cells (strain hela) derived from an epidermoid carcinoma of the cervix. *Journal of Experimental Medicine* **97**, (1953).
106. Almeqdadi, M., Mana, M. D., Roper, J. & Yilmaz, Ö. H. Gut organoids: Mini-tissues in culture to study intestinal physiology and disease. *Am J Physiol Cell Physiol* **317**, (2019).
107. Sato, T. *et al.* Single Lgr5 stem cells build crypt-villus structures in vitro without a mesenchymal niche. *Nature* **459**, (2009).
108. Sato, T. *et al.* Long-term expansion of epithelial organoids from human colon, adenoma, adenocarcinoma, and Barrett's epithelium. *Gastroenterology* **141**, (2011).
109. Yui, S. *et al.* Functional engraftment of colon epithelium expanded in vitro from a single adult Lgr5 + stem cell. *Nat Med* **18**, (2012).
110. Barker, N. *et al.* Lgr5+ve Stem Cells Drive Self-Renewal in the Stomach and Build Long-Lived Gastric Units In Vitro. *Cell Stem Cell* **6**, (2010).
111. Aihara, E. *et al.* Characterization of stem/progenitor cell cycle using murine circumvallate papilla taste bud organoid. *Sci Rep* **5**, (2015).

112. Huch, M. *et al.* In vitro expansion of single Lgr5 + liver stem cells induced by Wnt-driven regeneration. *Nature* **494**, (2013).
113. Kim, M. *et al.* Patient-derived lung cancer organoids as in vitro cancer models for therapeutic screening. *Nat Commun* **10**, (2019).
114. Greggio, C. *et al.* Artificial three-dimensional niches deconstruct pancreas development in vitro. *Development (Cambridge)* **140**, (2013).
115. Drakhlis, L. *et al.* Human heart-forming organoids recapitulate early heart and foregut development. *Nat Biotechnol* **39**, (2021).
116. Lee, J. *et al.* Hair-bearing human skin generated entirely from pluripotent stem cells. *Nature* **582**, (2020).
117. Biton, M. *et al.* T Helper Cell Cytokines Modulate Intestinal Stem Cell Renewal and Differentiation. *Cell* **175**, (2018).
118. Nozaki, K. *et al.* Co-culture with intestinal epithelial organoids allows efficient expansion and motility analysis of intraepithelial lymphocytes. *J Gastroenterol* **51**, (2016).
119. Heuberger, C. E. *et al.* MHC class II antigen presentation by intestinal epithelial cells fine-tunes bacteria-reactive CD4 T cell responses. *Mucosal Immunol* (2023) doi:10.1016/j.mucimm.2023.05.001.
120. Noel, G. *et al.* A primary human macrophage-enteroid co-culture model to investigate mucosal gut physiology and host-pathogen interactions. *Sci Rep* **7**, (2017).
121. Na, Y. R. *et al.* Prostaglandin E2 receptor PTGER4-expressing macrophages promote intestinal epithelial barrier regeneration upon inflammation. *Gut* **70**, (2021).
122. Read, E., Jowett, G. M., Coman, D. & Neves, J. F. Co-Culture of Murine Small Intestine Epithelial Organoids with Innate Lymphoid Cells. *Journal of Visualized Experiments* **2022**, (2022).
123. Baumdick, M. E. *et al.* HLA-DP on Epithelial Cells Enables Tissue Damage by NKp44+ Natural Killer Cells in Ulcerative Colitis. *Gastroenterology* **165**, (2023).
124. Boye, T. L., Steenholdt, C., Jensen, K. B. & Nielsen, O. H. Molecular Manipulations and Intestinal Stem Cell-Derived Organoids in Inflammatory Bowel Disease. *Stem Cells* vol. 40 Preprint at https://doi.org/10.1093/stmcls/sxac014 (2022).

125. Howell, K. J. *et al.* DNA Methylation and Transcription Patterns in Intestinal Epithelial Cells From Pediatric Patients With Inflammatory Bowel Diseases Differentiate Disease Subtypes and Associate With Outcome. *Gastroenterology* **154**, (2018).
126. Arnauts, K. *et al.* Ex Vivo Mimicking of Inflammation in Organoids Derived From Patients With Ulcerative Colitis. *Gastroenterology* **159**, (2020).
127. d'Aldebert, E. *et al.* Characterization of Human Colon Organoids From Inflammatory Bowel Disease Patients. *Front Cell Dev Biol* **8**, (2020).
128. Chang, X. *et al.* Macrophage-derived exosomes promote intestinal mucosal barrier dysfunction in inflammatory bowel disease by regulating TMIGD1 via mircroRNA-223. *Int Immunopharmacol* **121**, (2023).
129. Hammoudi, N. *et al.* Autologous organoid co-culture model reveals T cell-driven epithelial cell death in Crohn's Disease. *Front Immunol* **13**, (2022).
130. Robinson, J. P. Flow cytometry: past and future. *BioTechniques* vol. 72 Preprint at https://doi.org/10.2144/btn-2022-0005 (2022).
131. Shapiro, H. M. The Evolution of Cytometers. *Cytometry Part A* vol. 58 Preprint at https://doi.org/10.1002/cyto.a.10111 (2004).
132. Ferrer-Font, L. *et al.* Panel Design and Optimization for High-Dimensional Immunophenotyping Assays Using Spectral Flow Cytometry. *Curr Protoc Cytom* **92**, (2020).
133. Schmutz, S., Valente, M., Cumano, A. & Novault, S. Spectral cytometry has unique properties allowing multicolor analysis of cell suspensions isolated from solid tissues. *PLoS One* **11**, (2016).
134. Sahir, F., Mateo, J. M., Steinhoff, M. & Siveen, K. S. Development of a 43 color panel for the characterization of conventional and unconventional T-cell subsets, B cells, NK cells, monocytes, dendritic cells, and innate lymphoid cells using spectral flow cytometry. *Cytometry Part A* (2020) doi:10.1002/cyto.a.24288.
135. Futamura, K. *et al.* Novel full-spectral flow cytometry with multiple spectrally-adjacent fluorescent proteins and fluorochromes and visualization of in vivo cellular movement. *Cytometry Part A* **87**, (2015).
136. Keenan, M. R., Timlin, J. A., Van Benthem, M. H. & Haaland, D. M. Algorithms for constrained linear unmixing with application to the

hyperspectral analysis of fluorophore mixtures. in *Imaging Spectrometry VIII* vol. 4816 (2002).

137. Larsen, A. K. *et al.* Autofluorescence in freshly isolated adult human liver sinusoidal cells. *Eur J Histochem* **65**, (2021).
138. Croce, A. C. *et al.* Human liver autofluorescence: An intrinsic tissue parameter discriminating normal and diseased conditions. *Lasers Surg Med* **42**, (2010).
139. Roederer, M. Spectral compensation for flow cytometry: Visualization artifacts, limitations, and caveats. *Cytometry* **45**, (2001).
140. Heubeck, A. *et al.* Cross-platform immunophenotyping of human peripheral blood mononuclear cells with four high-dimensional flow cytometry panels. *Cytometry Part A* **103**, (2023).
141. Jalali, S. *et al.* A high-dimensional cytometry atlas of peripheral blood over the human life span. *Immunol Cell Biol* **100**, (2022).
142. Park, L. M., Lannigan, J. & Jaimes, M. C. OMIP-069: Forty-Color Full Spectrum Flow Cytometry Panel for Deep Immunophenotyping of Major Cell Subsets in Human Peripheral Blood. *Cytometry Part A* **97**, (2020).
143. Pierzchalski, A., Zenclussen, A. C. & Herberth, G. OMIP-94: Twenty-four-color (thirty-marker) panel for deep immunophenotyping of immune cells in human peripheral blood. *Cytometry Part A* **103**, (2023).
144. Reichard, A. & Asosingh, K. Best Practices for Preparing a Single Cell Suspension from Solid Tissues for Flow Cytometry. *Cytometry Part A* **95**, (2019).
145. Liu, Z., Gu, Y., Shin, A., Zhang, S. & Ginhoux, F. Analysis of Myeloid Cells in Mouse Tissues with Flow Cytometry. *STAR Protoc* **1**, (2020).
146. Haubruck, P. *et al.* Flow cytometry analysis of immune cell subsets within the murine spleen, bone marrow, lymph nodes and synovial tissue in an osteoarthritis model. *Journal of Visualized Experiments* **2020**, (2020).
147. Jameson, V. J. *et al.* Unlocking autofluorescence in the era of full spectrum analysis: Implications for immunophenotype discovery projects. *Cytometry Part A* **101**, (2022).
148. Yu, Y. R. A. *et al.* Flow cytometric analysis of myeloid cells in human blood, bronchoalveolar lavage, and lung tissues. *Am J Respir Cell Mol Biol* **54**, (2016).

149. Stankovic, B. *et al.* Immune Cell Composition in Human Non-small Cell Lung Cancer. *Front Immunol* **9**, (2018).
150. Brownlie, D. *et al.* Accumulation of tissue-resident natural killer cells, innate lymphoid cells, and CD8+ T cells towards the center of human lung tumors. *Oncoimmunology* **12**, (2023).
151. Caër, C. *et al.* TREM-1+Macrophages Define a Pathogenic Cell Subset in the Intestine of Crohn's Disease Patients. *J Crohns Colitis* **15**, (2021).
152. Krabbendam, L., Nagasawa, M., Spits, H. & Bal, S. M. Isolation of Human Innate Lymphoid Cells. *Curr Protoc Immunol* **122**, (2018).
153. Wiggins, B. G. *et al.* The human liver microenvironment shapes the homing and function of CD4+ T-cell populations. *Gut* **71**, (2022).
154. Filipovic, I. *et al.* 29-Color Flow Cytometry: Unraveling Human Liver NK Cell Repertoire Diversity. *Front Immunol* **10**, (2019).
155. Cheuk, S. *et al.* CD49a Expression Defines Tissue-Resident CD8+ T Cells Poised for Cytotoxic Function in Human Skin. *Immunity* **46**, (2017).
156. Alkon, N. *et al.* Single-cell analysis reveals innate lymphoid cell lineage infidelity in atopic dermatitis. *Journal of Allergy and Clinical Immunology* **149**, (2022).
157. Gualdrón-López, M. *et al.* Multiparameter Flow Cytometry Analysis of the Human Spleen Applied to Studies of Plasma-Derived EVs From Plasmodium vivax Patients. *Front Cell Infect Microbiol* **11**, (2021).
158. Goel, P., Acharya, S. & Ahuja, S. Flow cytometry in reactive lymph node aspirates: Evaluation of distribution of populations with immunophenotypic outliers. *Cytopathology* **33**, (2022).
159. Bondonese, A. *et al.* Impact of enzymatic digestion on single cell suspension yield from peripheral human lung tissue. *Cytometry Part A* **103**, (2023).
160. Snyder, M. E. *et al.* Human Lung-Resident Macrophages Colocalize with and Provide Costimulation to PD1hi Tissue-Resident Memory T Cells. *Am J Respir Crit Care Med* **203**, (2021).
161. Sasson, S. C. *et al.* Interferon-Gamma–Producing CD8+ Tissue Resident Memory T Cells Are a Targetable Hallmark of Immune Checkpoint Inhibitor–Colitis. *Gastroenterology* **161**, (2021).

162. Guo, N. *et al.* Immune subset-committed proliferating cells populate the human foetal intestine throughout the second trimester of gestation. *Nat Commun* **14**, (2023).
163. Sminia, T., Van Der Brugge-Gamelkoorn, G. J. & Jeurissen, S. H. M. Structure and function of bronchus-associated lymphoid tissue (BALT). *Critical Reviews in Immunology* vol. 9 Preprint at (1989).
164. Bienenstock, J. & McDermott, M. R. Bronchus- and nasal-associated lymphoid tissues. *Immunological Reviews* vol. 206 Preprint at https://doi.org/10.1111/j.0105-2896.2005.00299.x (2005).
165. Palkola, N. V. *et al.* Pathogen-specific circulating plasmablasts in patients with pneumonia. *PLoS One* **7**, (2012).
166. Mestecky, J. The common mucosal immune system and current strategies for induction of immune responses in external secretions. *J Clin Immunol* **7**, (1987).
167. Woof, J. M. & Mestecky, J. Mucosal Immunoglobulins. in *Mucosal Immunology: Fourth Edition* vols 1–2 (2015).
168. Bienenstock, J. *et al.* THE MUCOSAL IMMUNOLOGICAL NETWORK: COMPARTMENTALIZATION OF LYMPHOCYTES, NATURAL KILLER CELLS, AND MAST CELLS. *Ann N Y Acad Sci* **409**, (1983).
169. Sathaliyawala, T. *et al.* Distribution and Compartmentalization of Human Circulating and Tissue-Resident Memory T Cell Subsets. *Immunity* **38**, (2013).
170. Sathaliyawala, T. *et al.* Distribution and Compartmentalization of Human Circulating and Tissue-Resident Memory T Cell Subsets. *Immunity* **38**, (2013).
171. Niedzielska, M. *et al.* Differential gene expression in human tissue resident regulatory T cells from lung, colon, and blood. *Oncotarget* **9**, (2018).
172. Esendagli, G. *et al.* Malignant and non-malignant lung tissue areas are differentially populated by natural killer cells and regulatory T cells in non-small cell lung cancer. *Lung Cancer* **59**, (2008).
173. Ribot, J. C., Lopes, N. & Silva-Santos, B. γδ T cells in tissue physiology and surveillance. *Nature Reviews Immunology* vol. 21 Preprint at https://doi.org/10.1038/s41577-020-00452-4 (2021).

174. Meermeier, E. W. *et al.* Human lung-resident mucosal-associated invariant T cells are abundant, express antimicrobial proteins, and are cytokine responsive. *Commun Biol* **5**, (2022).
175. Gold, M. C. *et al.* Human mucosal associated invariant T cells detect bacterially infected cells. *PLoS Biol* **8**, (2010).
176. Greene, J. M. *et al.* MR1-restricted mucosal-associated invariant T (MAIT) cells respond to mycobacterial vaccination and infection in nonhuman primates. *Mucosal Immunol* **10**, (2017).
177. Cauley, L. S. *et al.* Cutting Edge: Virus-Specific CD4+ Memory T Cells in Nonlymphoid Tissues Express a Highly Activated Phenotype. *The Journal of Immunology* **169**, (2002).
178. Hogan, R. J. *et al.* Protection from respiratory virus infections can be mediated by antigen-specific CD4+ T cells that persist in the lungs. *Journal of Experimental Medicine* **193**, (2001).
179. Snyder, M. E. & Farber, D. L. Human lung tissue resident memory T cells in health and disease. *Current Opinion in Immunology* vol. 59 Preprint at https://doi.org/10.1016/j.coi.2019.05.011 (2019).
180. Kumar, B. V. *et al.* Human Tissue-Resident Memory T Cells Are Defined by Core Transcriptional and Functional Signatures in Lymphoid and Mucosal Sites. *Cell Rep* **20**, (2017).
181. Miron, M. *et al.* Human Lymph Nodes Maintain TCF-1hi Memory T Cells with High Functional Potential and Clonal Diversity throughout Life. *The Journal of Immunology* **201**, (2018).
182. Snyder, M. E. *et al.* Generation and persistence of human tissue-resident memory T cells in lung transplantation. *Sci Immunol* **4**, (2019).
183. Pizzolla, A. *et al.* Influenza-specific lung-resident memory t cells are proliferative and polyfunctional and maintain diverse TCR profiles. *Journal of Clinical Investigation* **128**, (2018).
184. Mei, H. E. *et al.* Plasmablasts With a Mucosal Phenotype Contribute to Plasmacytosis in Systemic Lupus Erythematosus. *Arthritis and Rheumatology* **69**, (2017).
185. Kutteh, W. H., Prince, S. J. & Mestecky, J. Tissue origins of human polymeric and monomeric IgA. *The Journal of Immunology* **128**, (1982).

186. Mora, J. R. & von Andrian, U. H. Differentiation and homing of IgA-secreting cells. *Mucosal Immunology* vol. 1 Preprint at https://doi.org/10.1038/mi.2007.14 (2008).
187. Mei, H. E. *et al.* Blood-borne human plasma cells in steady state are derived from mucosal immune responses. *Blood* **113**, (2009).
188. Allie, S. R. *et al.* The establishment of resident memory B cells in the lung requires local antigen encounter. *Nat Immunol* **20**, (2019).
189. Gutzeit, C., Chen, K. & Cerutti, A. The enigmatic function of IgD: some answers at last. *European Journal of Immunology* vol. 48 Preprint at https://doi.org/10.1002/eji.201646547 (2018).
190. De Grove, K. C. *et al.* Characterization and quantification of innate lymphoid cell subsets in human lung. *PLoS One* **11**, (2016).
191. Monticelli, L. A. *et al.* Innate lymphoid cells promote lung-tissue homeostasis after infection with influenza virus. *Nat Immunol* **12**, (2011).
192. Abel, A. M., Yang, C., Thakar, M. S. & Malarkannan, S. Natural killer cells: Development, maturation, and clinical utilization. *Frontiers in Immunology* vol. 9 Preprint at https://doi.org/10.3389/fimmu.2018.01869 (2018).
193. Wensink, A. C., Hack, C. E. & Bovenschen, N. Granzymes Regulate Proinflammatory Cytokine Responses. *The Journal of Immunology* **194**, (2015).
194. Duong, H. G. *et al.* Identification of CD81 T-Cell–Immune Cell Communications in Ileal Crohn's Disease. *Clin Transl Gastroenterol* **14**, (2023).
195. Metkar, S. S. *et al.* Human and Mouse Granzyme A Induce a Proinflammatory Cytokine Response. *Immunity* **29**, (2008).
196. Jonsson, A. H. *et al.* Granzyme K+ CD8 T cells form a core population in inflamed human tissue. *Sci Transl Med* **14**, (2022).
197. Müller, A. A. *et al.* An NK Cell Perforin Response Elicited via IL-18 Controls Mucosal Inflammation Kinetics during Salmonella Gut Infection. *PLoS Pathog* **12**, (2016).
198. Kägi, D., Odermatt, B. & Mak, T. W. Homeostatic regulation of CD8+ T cells by perforin. *Eur J Immunol* **29**, (1999).

199. Badovinac, V. P., Tvinnereim, A. R. & Harty, J. T. Regulation of antigen-specific CD8+ T cell homeostasis by perforin and interferon-γ. *Science (1979)* **290**, (2000).